Abstract

Research into the fibrillar structure of collagenous tissues is very important in the improvement of our understanding of various structural tissue defects.

The structure and properties of type I fibrillar collagen were studied by atomic force microscopy for use in conjunction with x-ray diffraction images in the development of a ptychography phasing algorithm. Various sample preparation methods were explored in relation to both imaging methods and the samples were characterised in terms of their suitability with respect to the ptychography algorithm and their implications for further research using the atomic force microscope.

A novel preparation method of rat-tail tendon samples for use with the AFM led to more realistic comparative images for use in the development of the three-dimensional ptychography algorithm due to the retention of the natural alignment of the samples. The images taken of highly aligned samples also expressed a squarer D-banding shape in comparison with past results using AFM, as well as sub-D-banding features that are comparable to data from TEM and SEM images of collagen fibrils.

The successful use of hydrated samples during x-ray diffraction led to the use of AFM imaging in liquid. Characterisation of histological sections of rat-tail tendons revealed fibril cross-sections that were available to the AFM tip and whose mechanical features could be further investigated using force-volume measurements on the AFM.

The imaging modes and contrast mechanisms used during the AFM imaging of the samples are discussed, taking into account the structural nature of collagen and the various effects that are known to be present in the imaging of samples using a scanning probe microscope.

Introduction

Although a large amount of research has been performed on it from the molecular level upwards, there is still much that is unknown with respect to the formation of fibril bundles as well as substructural details of the fibrils themselves [1][2].

The three dimensional organisation of type I collagen fibrils within a fibril bundle is currently being probed using x-ray diffraction imaging [3]. Atomic force microscope images have been used successfully in the past as a comparative model in the development of a two-dimensional ptychography phasing algorithm [2], the challenge now is to develop a three-dimensional phasing algorithm, again using AFM images as a comparative model. The AFM images produced during this report were used to do this, employing a range of approaches and novel preparation techniques were developed to produce images more suitable for this purpose.

The superficial structure of the collagen samples was also investigated during this project and variations in the shape of the characteristic D-banding of the fibrils was discussed in relation to past results from both electron microscopy techniques and AFM, as well as how the probe-nature of AFM as a technique may affect the images produced.

Collagen

Fibrous collagen is ubiquitous in vertebrates and forms the structural basis of all mammalian connective and supportive tissues, as well as being found in its mineralised form in bone and dentin. Collagen plays an important role in the storage and transmission of energy in the muscoskeleton due to its role in connective and structural tissue [4], this role is reflected in its high elastic properties as well as its high tensile strength [5]. There are over 27 genetically distinct types of collagen, its most common form being type I, which forms structures such as tendons, skin and bones [6][7]. It is type I collagen that is studied in this project, and was sourced from the tendons of rat-tails. Understanding the structure and properties of collagen is incredibly important for the treatment and research into various diseases such as Osteogenesis Imperfecta (‘brittle bone disease’) and Ehlers-Danlos syndrome (both disorders affecting type I collagen genesis in humans)[1][6][7].

At the molecular level, collagen is a right-handed triple helix composed of three left-handed polyproline II helices, which are in turn composed of proline, hydroxyproline and glycine in the sequence Gly-X-Y, with X and Y generally occupied by proline and hydroxyproline. The central domains of the polyproline chains fold into a tight right-handed helix (the polyproline II helix) due mostly to the steric repulsion between proline residues in the X-position and hydroxyproline residues in the Y-position. Peptide bonds form the backbone of the helix, leaving the amino acid side chains exposed. Due to the way the helix is folded, the glycine molecules will form an exposed line along the length of the helix; they will then make hydrogen bonds with the glycine molecules on the other two helices to form the right-handed triple helix with the hydroxyproline and proline molecules on the outside and the glycine molecules in the centre, forming a structurally strong core to the collagen molecule.

Two of the chains have identical amino acid sequences, but the third's sequence differs slightly. The structure of this molecule makes it incredibly strong, stable and rigid, and slight alterations in the sequencing (which is how the collagen type varies) can give it the ability to make use of its roles in cell adhesion, tissue regulation and infrastructure and determination of cell phenotype [4][6][7].

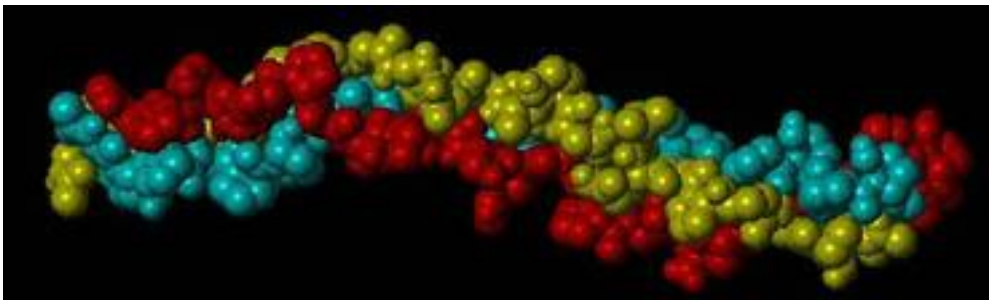

Fig 1
Model of type I molecular collagen, the individual polypeptide chains being indicated by different colours [4].

In vivo (and in specific conditions in vitro [8][9]), the collagen molecules self-assemble into a fibrillar structure and it has been proposed that they do this axially with a one quarter-staggered packing array – staggering themselves by approximately 22% of their length with respect to their nearest neighbour (see fig 2, below)[8]. It is this staggering that is said to give rise to the D-banding, which is visible under EM (electron microscopy), AFM, and X-ray diffraction imaging [2][6][7][10]. The length of the D-banding varies slightly between tissue types, eg. 67nm for tendon compared to 65nm for skin [4]. It is defined by two distinct regions: overlap (~20nm) and gap (~47nm) [8] see figure 2 – these two regions are caused by the staggering packing array, the gap region defined by an area where there is a space between the collagen molecules, and the overlap region where there is no space. Microfibrils, whose width is of the order of the collagen molecular width, will aggregate to make larger fibrils, which will in turn cross-link to form bundles called fibril bundles [8][11].

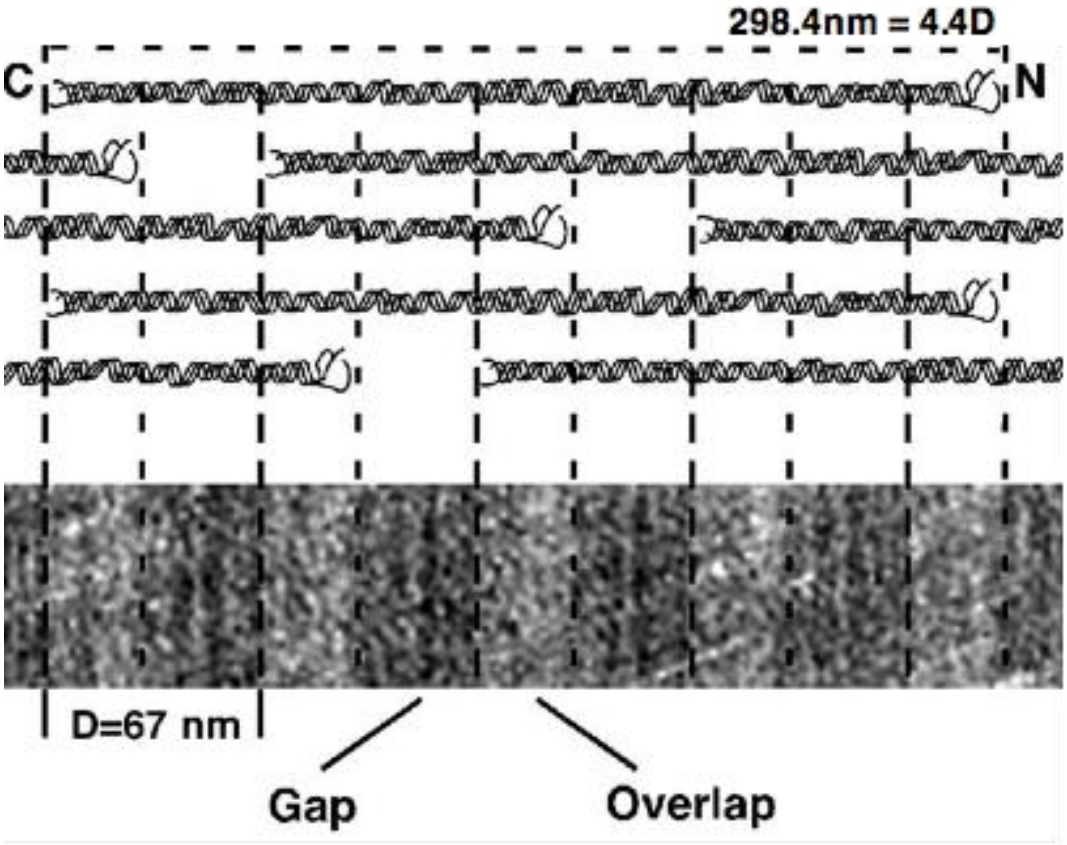

Fig 2
Illustration of the quarter staggered packing array of collagen molecules forming a fibril. Taken from [8].

A variation on this model has since been observed using x-ray diffraction. The model still involves a staggered distribution of the collagen molecules in the sub-fibrillar structure, but the collagen molecules are instead arranged in a supertwisted right-handed microfibril that interdigitates with neighbouring microfibrils to form a fibrillar superstructure. This microfibrillar structure is discontinuous, which will lea to "gap" and "overlap" type regions [11].

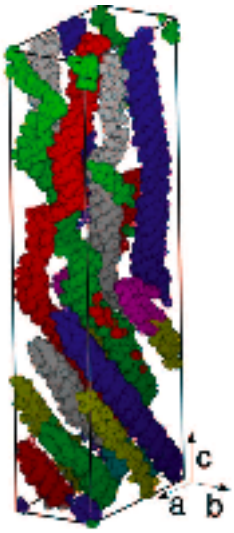

Fig 3
The 3D structure of a small section of the twisted microfibril is shown here with different collagen molecules indicated by different colours [11]

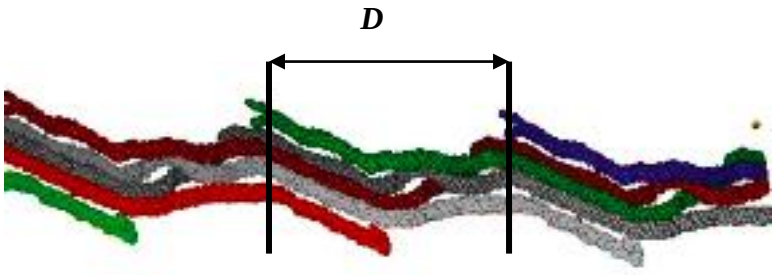

Fig 4
A larger section of the microfibril is shown with the periodic D-banding indicated [11]

It has been hypotesised that the microfibrils will then aggregate to form larger fibrils in the manner illustrated in figure 5. These fibrils can then cross-link to form fibril bundles.

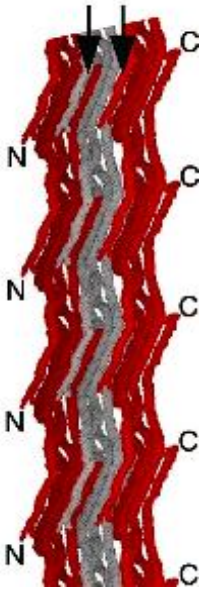

Fig 5
An illustration of the hypothesised sub-fibrillar structure, with the arrows indicating the individual microfibrils. [11]

Fibril bundles will then go on to form a wide range of collagenous tissues of different structural forms depending on their purpose. Tendon is rare in its structure, as the fibril bundles that make it up are incredibly well aligned with respect to one another and the direction of the tendon's length [12] (figure 6). The high level of alignment makes this particular sample suitable for use in x-ray diffraction experiments, as individual rows of fibrils can be resolved.

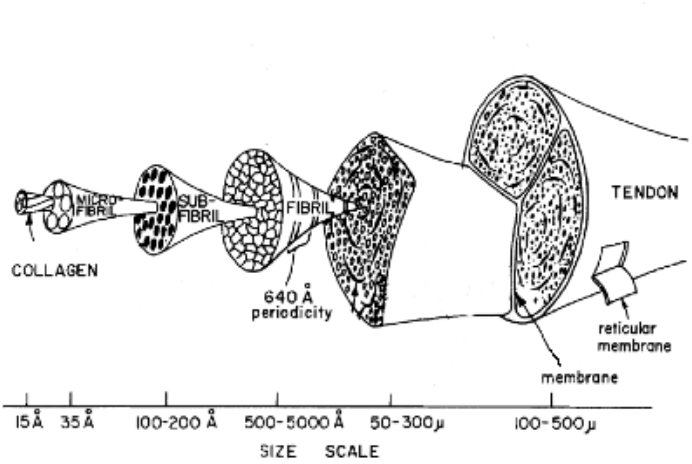

Fig 6
Illustration of the hierarchy of tendon from collagen molecule to whole tendon. Taken from [12]

Atomic Force Microscopy

The Atomic Force Microscope

The atomic force microscope (AFM) belongs to the family of scanning probe microscopes, which use a physical probe to scan a specimen and build up an image of its surface. The AFM uses a tip (usually silicon-nitrite or silicon-oxide) located at the end of a flexible cantilever attached to a much larger chip, which is in turn affixed to the microscope body. The cantilever is usually around 100μm long, with a shape dependent on the imaging mode being used, and the tip radius is ideally in the order of a few nanometres, but is often in the order of tens of nanometres. As the tip approaches the sample surface, the two begin to interact via long-range electrostatic and Van der Waals forces. The Van der Waals interaction can essentially be modelled by the Lennard-Jones potential (see figure 7), and describes the attractive interaction between atoms and molecules at short distances due to permanent and temporary dipole moments and the repulsive interaction at very short distances due to the electrostatic repulsion between the electrons as well as the force due to the Pauli Exclusion Principle. In dry conditions, the tip will also be affected by the capillary forces due to the water condensed on both the tip and sample surface, of which there will always be a non-negligible amount. The mechanical properties of the sample surface will also play a role in the tip-sample interaction, although both these contributions become more prominent when the tip starts to be scanned across the material, i.e. when imaging begins [13][14].

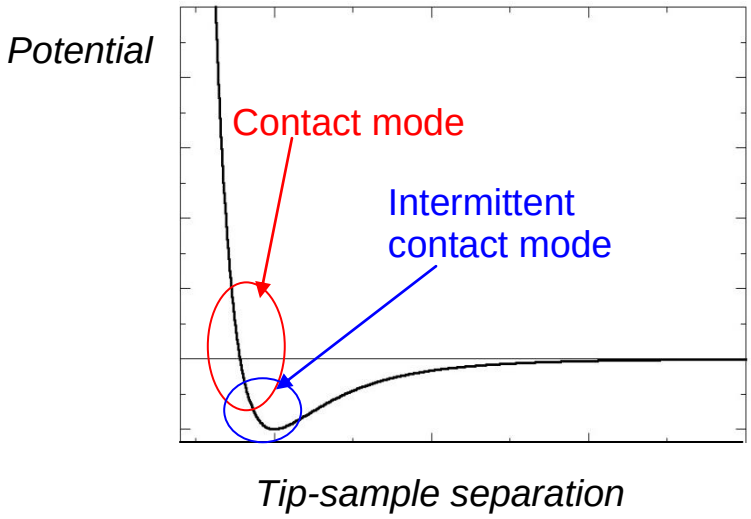

Fig 7
Illustration of the interaction between the tip and the sample as a function of distance, with the regions in which various imaging modes operate highlighted.

When the tip is in contact with the sample surface it is raster scanned along the surface of the sample being imaged. The strength of the interaction between the tip and the sample is measured by observing the cantilever deflection: a laser spot is shone onto its reflective upper side, which shines it onto a four-part photodiode, this then measures both the vertical and lateral deflection of the cantilever by comparing

the sum of the energy incident on each photodiode. The experimenter aims to keep the average interaction strength constant. To do keep this constant interaction strength P.I.D. (proportional-integral-derivative) feedback loop is employed to control the extension and contraction of a piezo tube attached to either the probe or the base of the sample (in this case the piezo was attached to the probe – see appendix 3) which controls the distance between the chip bearing the cantilever and the microscope base. The piezo extension and contraction is recorded and will reflect the topography of the sample[13][14].

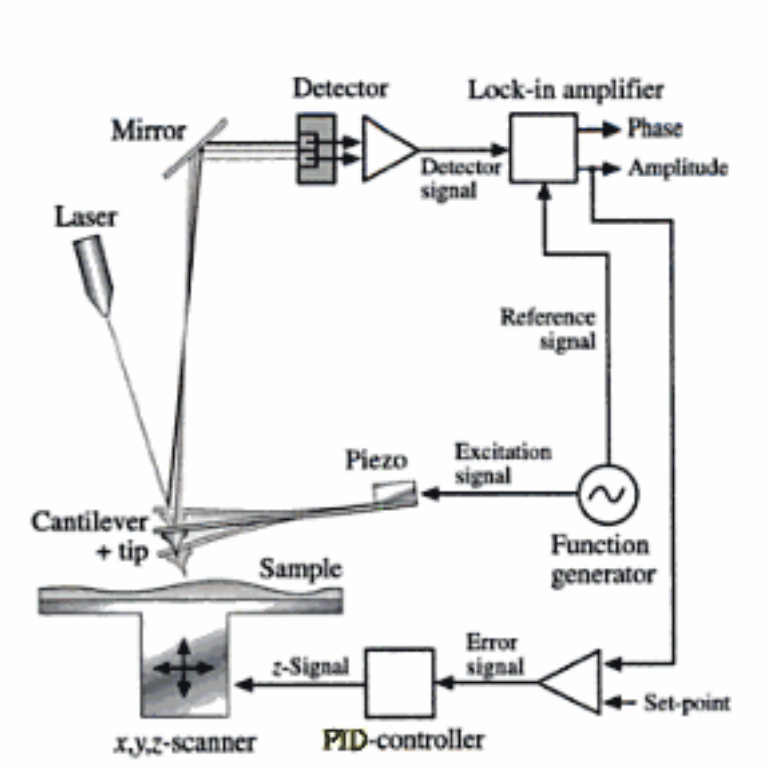

Fig 8
Schematic of the AFM function (in intermittent contact mode) and instrumentation [14]

Imaging modes

There are a wide range of different imaging modes that can be used in AFM. During this project contact and intermittent contact modes were exclusively used, with the majority of the work being done in intermittent contact mode. As such, these are the two modes that will be discussed during this introductory explanation.

Contact mode

This is the simplest and most commonly used mode in AFM. The cantilever is kept in the repulsive regime, with a distance of less than a few angstroms above the sample surface [13][14]. One can imagine this imaging mode like a person reading Braille: their finger scans across each line of text in turn from left to right, constantly sensing any change in topography.

As the tip is scanned across the sample surface, its deflection is kept constant in the way described in the previous section; the larger the deflection, the harder the tip is 'pressing' on the sample surface (i.e. the higher the interaction strength between the itp and the sample) and hence the higher the resolution of the resultant image, but the higher the risk of damaging the sample surface. The cantilevers required for this

imaging mode generally have a low force constant, usually in the order of 0.1N/m, as the tip needs to be easily deflected so that small features can be seen and so the sample surface will not be damaged. This imaging mode is useful for samples with hard surfaces, as it is quick and easy to perform and such surfaces will not be easily damaged [13][14].

There are various unknown parameters in this imaging mode, and these are also relevant in the other modes that the AFM operates in. Firstly, the distance between the tip and sample is not precisely known; the interactions between tip and sample can be quite long ranging and will vary between sample and tip materials, so only an average distance can be given. When the interaction is kept in the repulsive regime of the force curve, the tip can be modelled as being in "real contact" with the surface – the relationship between force and tip-sample separation should be approximately proportional, so the images gained are reliable depictions of the surface and can be analysed. At the same time the very nature of this "contact" is disputable and dependent on the nature of the interactions between the tip and the sample – whether they be due to electrostatic interaction or the Pauli Exclusion Principle. The basic Van der Waals interactions upon which the model of the AFM is based are themselves subject to the chemical properties of the sample and tip, such as relative charge distribution across the sample surface – the presence of which can give the appearance of topographical surface features where there are none. To analyse this, the relative charge of the tip also has to be considered [13][14][15][16].

The tip of the cantilever is always charged due to its interaction with the water condensed on its surface, of which there is always a non-negligible amount. The nature of the interaction, and hence the resultant charge of the tip, is described by the pI of the material that the tip is made of. In this way the tip will interact with the sample differently depending on its material and the relative charge distribution on the sample surface.

Intermittent contact mode

This mode can be modelled on the equilibrium area of the Lennard-Jones potential; the cantilever is oscillated at a frequency close to its resonant frequency and then scanned across the sample surface. The oscillations of the cantilever will have amplitudes in the order of 10nm and the tip will effectively "tap" the sample as it moves across its surface, hence dissipating energy, which damps its oscillations. The experimenter will define a setpoint for the amplitude and the piezo will move the chip to keep this constant – this should keep the energy dissipated (and hence the force incident) on the sample surface constant. The piezo's movement is again monitored and will reflect the surface's topography. The cantilevers used in this imaging mode are generally very stiff ("beam-shaped"), so that the tip can escape the capillary force caused by the water condensed on the sample's surface [13][14][15].

This imaging mode is useful for delicate samples, as the lateral forces on the sample surface are far lower than those experienced in contact mode. This mode can also give an image based on the phase difference between the cantilever and the driver as the tip is scanned across the sample surface [13][14].

The phase signal is very sensitive to changes in tip-sample separation, tip-sample interaction area and the viscoelastic properties of the sample surface. It shows very little dependency on the "softness" of the sample, which is dependent on the strength of the repulsive force between the sample and the tip when they are in "contact" [4]. The final phase image will be a convolution of all these contributions, which become very hard to differentiate. If the experimenter is imaging a sample with very little topographical variation, but a larger variation in viscoelastic properties, the phase image can be very helpful, although the resultant data given will generally be of qualitative value rather than quantitative [13][14][15].

As intermittent contact mode was used most extensively throughout this project, I shall discuss the tip-sample surface interaction a little further.

At large distances from the sample surface, the cantilever and tip can be modelled as a mass on a spring, with a spring constant dependent on the cantilever material and dimensions. When forced into oscillation, the cantilever's motion can be described as a driven harmonic oscillator to a good approximation – see figure 9 [13][14][15].

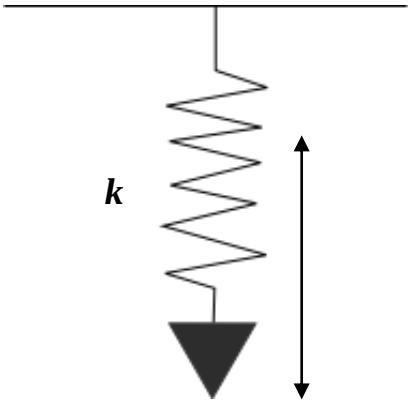

Fig 9
Model for non-interacting tip at full extension – spring constant = ***k***

As the tip approaches the surface the two will begin to interact, with the tip being subject to either attractive or repulsive forces. These forces can be modelled like a second spring, the stronger the attractiveness of the interactions the higher this second spring constant will be – see figure 10 [13][14][15].

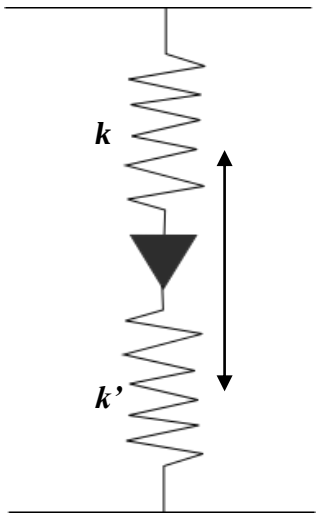

Fig 10
Model for tip interacting with the surface – overall spring constant = ***k + k'***

This interaction will change the potential energy of the cantilever's oscillations and its resonant frequency will increase accordingly. This effect is due to Van der Waals interaction as well as any long-range electrostatic forces between the tip and the sample surface and will be affected by the chemical nature of the atoms and molecules that make up the sample surface. While the tip is in contact with the sample surface it will begin to experience repulsive forces due to various interactions, such as the electron-electron repulsion as the two molecular shells approach one another, and the force due to the Pauli Exclusion Principle as the electronic orbitals begin to overlap. The higher these repulsive forces are, the stiffer the sample and the higher the damping experienced by the cantilever. This dependence of the amplitude on the surface charge of the sample becomes particularly important when we consider the relative charge over various regions on the sample's surface [13][14].

The frequency of the interacting tip will vary according to the equation

$f = (1/2\pi)\sqrt{(k/m)}$ [16]

The amplitude will be damped according to the energy dissipated on the sample surface.

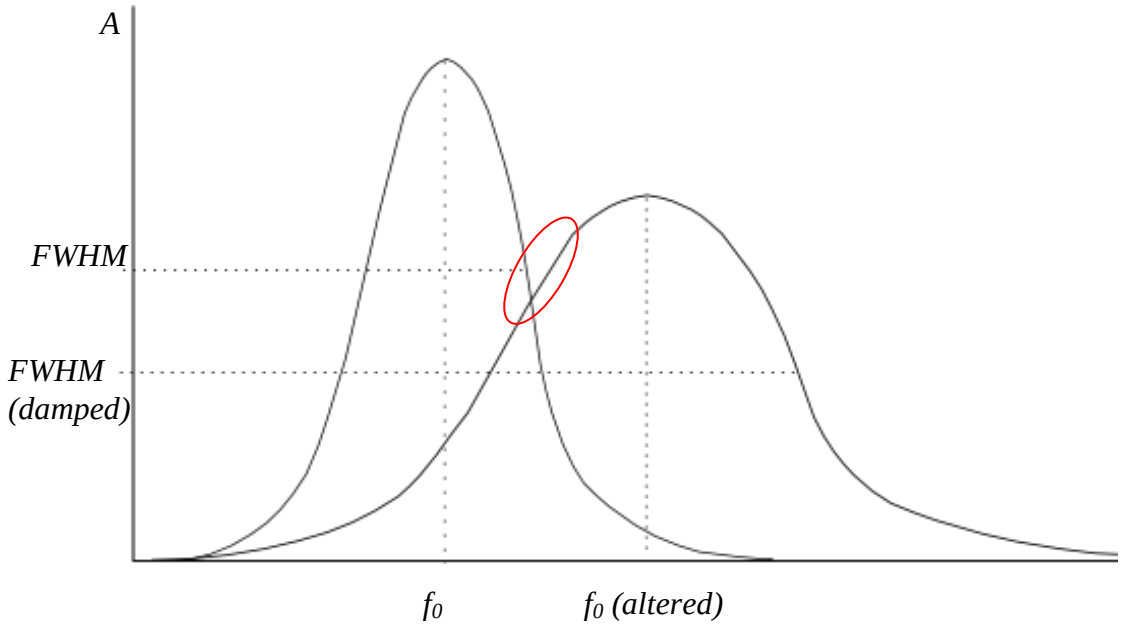

Fig 11
Illustration of how the resonance curves of the resonance curve of the cantilever varies as it begins to interact with the sample. The red ellipse highlights the target amplitude region, which is set before the resonance peak so that the oscillation to not go out of control and break the cantilever [13][14].

The amplitude peak of the resonance curve corresponds to a phase difference of $(-\pi/2)$, which is generally the region of the phase curve with the highest gradient. When the cantilever begins to interact with the sample, the phase curve will be shifted up the frequency range, just as the amplitude curve was, and will be "flattened" due to the damping of the oscillation [13][14][15].

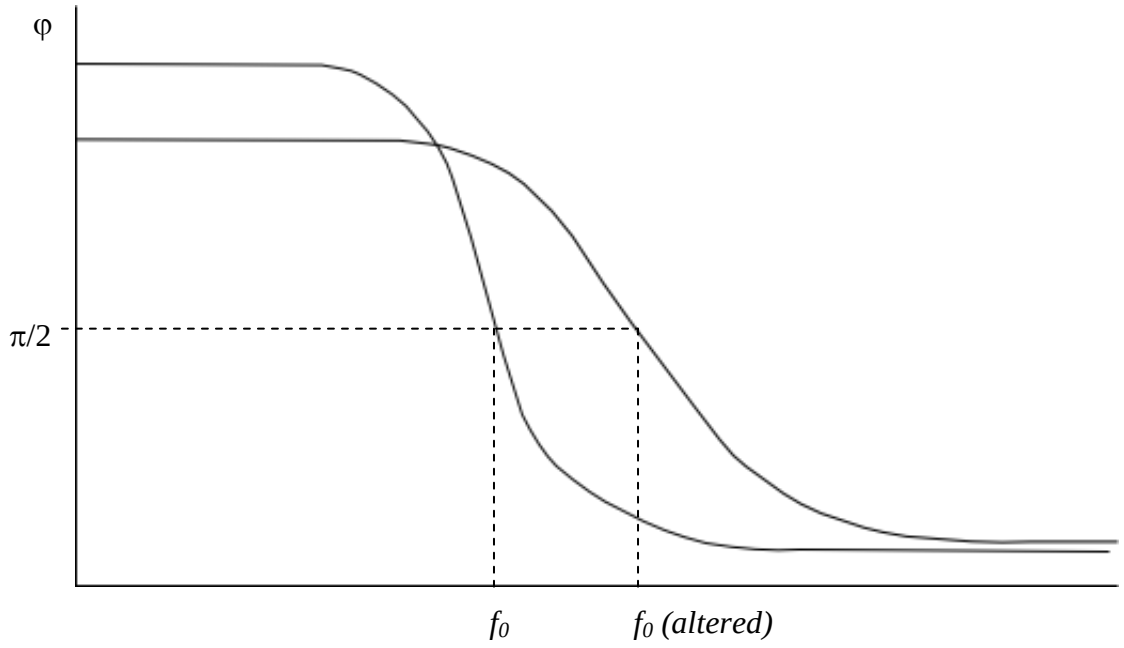

Fig 12
Illustration of the phase curve of an interacting and non-interacting tip in oscillation.

The 'error' signal

Each of the imaging modes can also produce an image based on the 'error signal'. This is the signal used by the PID feedback loop to control the extension and contraction of the piezo as it moves over the sample surface. The resultant signal is a transformation of the laser-spot deflection as the tip encounters surface features. This signal is particularly sensitive to sudden variations in the topography of the sample surface, as the PID feedback loop has less time to react to the signal compared to a smoother gradient. The resultant signal is particularly sensitive to the derivative part of the transformation, but will essentially be a convolution of the proportional, integral and derivative parts[13][14].

Amplitude image

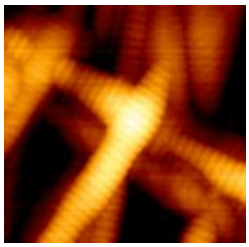

Height image

Figs 13, 14
Illustration of the visual difference between the amplitude and height images of the same area of a collagen sample, taken using intermittent contact mode.

Unfortunately, as this is only the error signal, this image cannot be used to analyse the sample to any large degree – the information used is a transformation of the real topography. It is a useful aid to visualising the sample surface, as well as recognising any key features of its surface, whose positions in the x-y plane will be valid. In this project the error signal is often used in conjunction with the development of the ptychography algorithm, as the images show the position and length of the D-banding

clearly – these images will still be valid for use as a comparative model in the development of the ptychography algorithm as they still show the position of feature edges on the x-y plane [13][14].

Tip Effects

Due to the probe nature of atomic force microscopy, the images gained will be a convolution of the tip shape and the surface features. Ideally the tip should have a radius of a few nanometres and be pyramidal or conical in form, so the convolution will be negligible as the surface features would be far larger. Unfortunately this is not generally the case, especially after the tip as been used. A tip may be unintentionally manufactured so that it is misshapen, for example it may have two apices giving a "double tip" effect, or may simply be blunter than specified (this is generally the case). After use a tip will generally become blunter and more misshapen, and may pick up parts of looser and softer samples, all of which contribute to the inaccurate representation of the sample surface topography.

During the imaging the experimenter will aim to minimise the effects of the tip shape and be able to recognise when the sample surface is exhibiting a real feature and when the feature being seen is due to a tip effect.

Convolution of surface topography

As all tips are either conical or pyramidal in form, rather than Dirac peak-like, a larger area of the tip will interact with the sample surface when surface features are encountered. This increase in sample-tip interaction area will increase the total interaction strength between the tip and the sample, and any surface features will become a convolution of the feature and the tip gradient [13][14].

This effect, illustrated in figure 15, is minimised by having a tip with as high an aspect ratio as possible, but will always be present in all the AFM imaging modes.

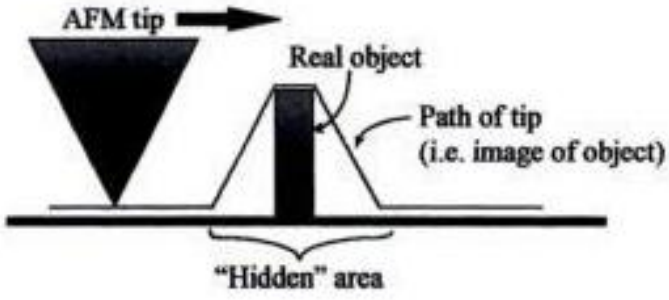

Fig 15
Figure illustrating the effect of tip-sample convolution, taken from [13]

Misshapen tips

If a misshapen tip is being used and it is scanned in intermittent contact mode across a harder surface without much topographical variation, the effect is obvious- it would seem that there is a motif repeated across the surface, which actually corresponds to the shape of the tip [13].

When scanning across a rougher surface a similar effect can be seen by the more experienced experimenter who knows the general form of the sample surface being imaged – the surface features will be distorted by the tip-shape:

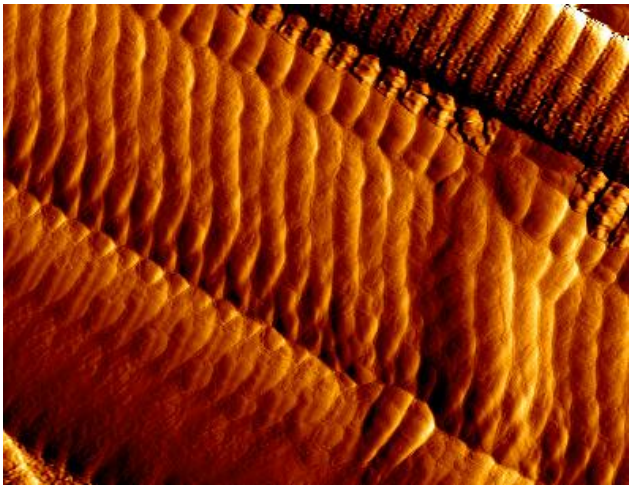

Fig 16
This image shows a collagen fibril – running along the centre of the image - whose D-banding (which should run perpendicular to its length) has been distorted by a misshapen tip.

If sample artefacts are picked up during the scan a similar effect may be seen. If the general sample surface is unknown it is essential to use a few different tips to make sure that the resultant image is reliable.

If working with a "double tip" the effect will not be observable across a smoother surface, but once a feature is encountered. Its feature edges will be repeated, often partway through the original feature:

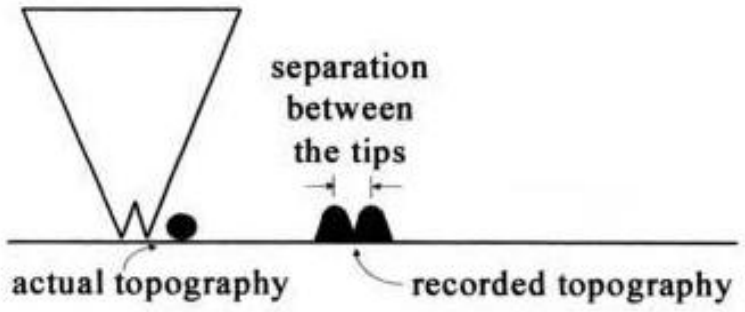

Fig 17
Diagram illustrating the double tip effect, taken from [13]

The tip shape can be analysed using a specialised sample called a "TipCheck", which has spikes randomly placed across its surface, each with a radius in the order of a nanometre and a very high aspect ratio – such that they can be considered as Dirac peaks when compared to the size of the tip [REF]. This sample surface will then image the tip, rather than the other way around. The resultant image will be processed such that the average shape of the tip (which is repeated each time it taps the surface) is taken and deconvolved with respect to the sample-surface.

X-ray diffraction imaging - ptychography

Thus far the three dimensional structure of a fibril bundle is not fully known, in particular how the fibrils order themselves with respect to one another and how they "touch". To further investigate this feature of the assembly of collagen in living tissue, x-ray diffraction images have been taken of native rat-tail collagen [2][12].

As with other conventional scattering techniques, the phase information in the scattered wave is inherently lost when its intensity is measured. The phase must be found in order to determine the electron intensity distribution along the axial D-banding of the collagen and hence reconstruct its real-space structure, as it is essential in the computation of an inverse Fourier transform, which converts the information from reciprocal to real space[2].

The approach being used in conjunction with this project is that of ptychography, which employs oversampling of a field of view restricted specimen. The intensity of adjacent peaks is easily recorded and the intensity of their midpoint, referred to as the oversampled diffraction spots, gives a measure of their relative phase. By moving the x-ray beam less than one unit cell a new measure can be obtained for this phase difference and hence all phases can be obtained unambiguously [18]. An iterative algorithm is being developed to do this.

The AFM images that were obtained throughout this project were used as a model to simulate the diffraction patterns that would be found from real data, which are then used to reconstruct the original specimen image [3].

Materials and Methods

Sample preparation – Atomic Force Microscopy

Hand prepared samples

During this project native rat-tail collagen was almost exclusively used, with some imaging performed on compressed collagen gel derived from rat-tail collagen. The tail of a rat consists of the end of the spine, which reaches partway down the tail, surrounded by about five tendons, which carry on past the end of the tailbone. The

tendons are attached to one another and to the bone by connective tissue such as cartilage and collagenous membrane. Each tendon is around 1cm in diameter and is made up of fibril bundles of about 100μm in diameter; these fibril bundles are themselves very well aligned within the tendon (running parallel to the tendon's length) and are constructed of incredibly well aligned collagen fibrils (although their exact three dimensional structure is unknown), each being about 1μm in diameter [12]. This feature of rat-tail collagen is very important for its use in ptychography, as very well aligned samples are needed to gain a clear diffraction pattern that can be analysed to find the internal structure of the fibril bundle. Because of this, many of the samples were prepared in such a way as to keep the fibrils as well aligned as possible. This proved to be quite difficult as the membrane that kept the fibril bundles together had to be removed before the sample could be probed by the AFM and the fibrils would immediately splay.

The rat-tails used were stored whole in the freezer after removal from the animal so as to prevent their degradation, they were thawed just before dissection to facilitate the process. The dissection is performed using a surgical scalpel and sharp surgical tweezers, which must be kept as sharp and possible so that the incisions are clean and the fibril bundles do not become attached to the tweezer ends (which they easily do, given tweezers whose ends have been contorted in any way). The instruments must also be cleaned with ethanol prior to use, so as to keep sample contamination to a minimum. To begin the dissection, the skin surrounding the tail must be removed: the hilt of the tail is cut off using a scalpel, and an incision is made along the skin, running the length of the tail. The skin of the tail is then peeled back, cutting and removing any connective tissue attaching it to the tendons. The tendons are attached to the vertebrae periodically along the length of the tail by cartilage; these joins are cut carefully with the scalpel while the tendons are individually pulled away from the tailbone and the other tendons using surgical tweezers. Although the fibril bundles in the tendon will naturally start to come away from the tendon, each tendon should be kept as intact as possible during this process, so that the fibril bundles within them do not split and splay the collagen fibrils, ruining the alignment. Any fat or other debris on the tendons is removed using tweezers and the scalpel. The fibril bundles can now either be separated or if any tendons are still very much intact they can be stored whole – depending on the samples that are required. For AFM imaging, the fibril bundles needed to be separated, but some of the diffraction experiments required whole sections of tendon to be used (albeit rather small sections from the tendon tip).

The extracted fibril bundles (or whole tendon) are then rinsed with deionised water to remove contaminants and stored in a small container (such as an eppendorf) in a PBS/Azide solution. The PBS (phosphate buffered saline) is a buffer solution and the azide kills any bacteria so that the collagen doesn't degrade, although if vascular tissue is left in, the collagen will still rot.

The collagen fibril bundles kept in this solution will survive for up to six months, but the crosslinking between the collagen fibrils will start to lose its integrity. This process actually aids standard AFM sample preparation, as it is easier to separate the fibrils from the fibril bundle.

The collagen is prepared for AFM imaging by taking a small section (~1cm in length) of a single fibril bundle (this will contain hundreds of fibrils [12]), rinsing it in

deionised water to remove any PBS, which will crystallise when dried, then laid on a glass substrate, whose surface has been cleaned with ethanol. The fibril bundle itself is too thick for AFM imaging, and the bundle is held together by a surrounding membrane, which will prevent the AFM probe from interacting with the fibril surface [12][13][14], this means the fibril bundle must be opened and then flattened before imaging. For most imaging purposes there is no need to keep the collagen aligned and so the easiest way to prepare it is to simply spread the fibrils out across the surface of the glass substrate, before letting them dry (see figure 18). This will give clear images of the structure of the individual fibrils and this technique was used for training on the AFM and familiarisation with the samples themselves, but for use with the algorithm the fibrils must be aligned. To keep areas of natural alignment the fibril bundle was laid on the glass surface, the membrane was removed by delicately moving the tweezer ends along the sample's surface in a motion parallel to its length. The fibrils were then "pulled" (but not stretched) across the substrate surface in the direction of the bundle's length. A confocal microscope can be used to make the process easier, and to make sure that there will definitely be aligned areas in the sample (see figure 19).

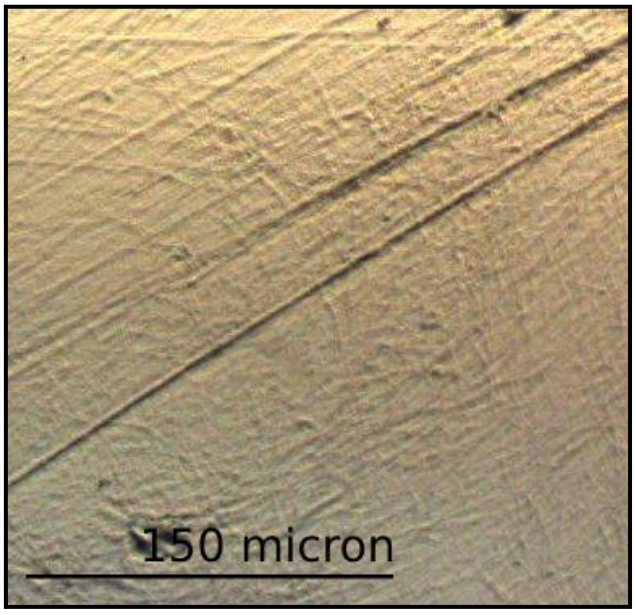

Fig 18
Smeared fibril section shown under the confocal optical microscope.

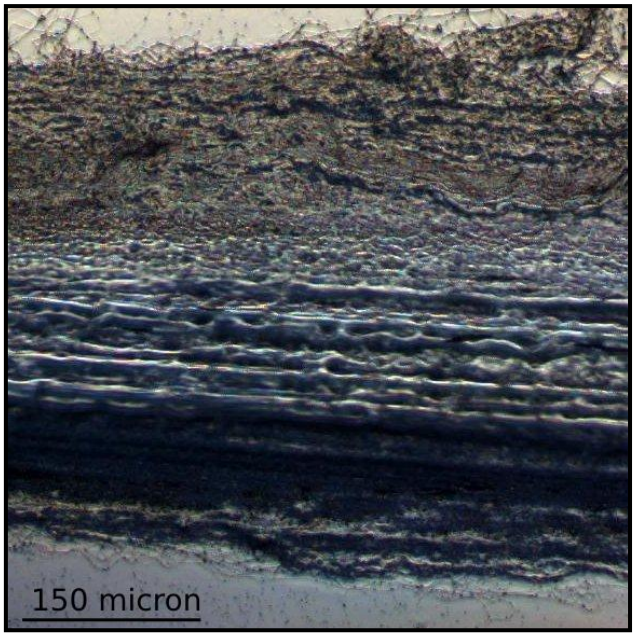

Fig 19
Aligned section of a fibril bundle shown under the confocal microscope. Areas of alignment are shown in the central region of the section.

If the imaging is to be done in air, the sample will then be either left to dry or can be dried using a Nitrogen air-gun to speed up the process. These samples can then be stored for several months before any degradation is noticeable.

Before imaging in liquid the samples were rehydrated, with a buffer solution, by pipetting the solution directly onto the sample and substrate. The wet sample is then left for a short amount of time (under a minute) to fully rehydrate before imaging

Histological Section Preparation Protocol

Another approach was taken to preserve the natural alignment of the fibril bundles within the tendon during imaging for use with both AFM and XRD in the preparation of histological sections.

These sections are generally prepared for pathological examination under an optical microscope of biopsied tissues [19].

Fixation
After a sample of tissue has been removed from an organism, the cells within it start to die and the integrity of the tissue structure starts to break down, thus making it useless for pathological analysis, etc. To stop this process, the tissue sample needs to be 'fixed'. The most common fixation techniques involve aldehydes [REF] such as formalin (formaldehyde in phosphate buffered saline) or glutaraldehyde. These substances fix by cross-linking proteins, and so although a fixation process that uses the aldehydes preserves the structural integrity of the tissue, it will also damage its biological functionality – for example the function of enzymes – as well as altering its mechanical properties. Alcohols can be used as fixatives in much the same way, but will harden the tissue, sometimes to the point of brittleness.

Freezing the sample is another option, as it stops autolysis and putrification processes and maintains cellular integrity; unlike the aforementioned methods, snap freezing in liquid nitrogen or solid carbon dioxide will not damage the tissue's potential for biological function or change its mechanical responses after thawing.

Dehydration and infiltration
The histological sections that are prepared from the tissue sample must be very thin – in the order of microns - so that they are usable for pathological examination. To facilitate this sectioning, the tissue sample must be embedded in a hard medium that permeates the entire sample. The most common medium used for this purpose is paraffin wax, but before the wax can be driven into the sample, the water that resides in the sample must be driven out, i.e. the sample must be dehydrated. This is done using progressively more concentrated alcohol solutions, after which a clearing agent (e.g. xylene) is used to remove the alcohol, then the molten wax finally replaces the clearing agent. For harder samples and thinner sections, a plastic resin is used. If a sample is frozen, it is simply sectioned while frozen.

Sectioning
Sections are cut from the wax block using a microtome; the most common types are the rotary and the sledge. Sections are often cut one after the other, sticking end to end and creating a "ribbon" of sections. These are then floated on a warm water bath, which smoothes out the wax and enables their adhesion onto glass slides. An additional adhesive is often needed for very hard or very soft samples.

Frozen sections are cut on a machine called a cryostat – a microtome, usually a rotary, in a deep freeze cabinet, so that all stages from sample selection to sectioning are carried out at -20°C or lower. Collagen sections can then be kept at around 5ºC, as they will degrade at the same rate as the sections described earlier.

Staining
A sectioned sample will generally be stained to give the varying tissue types contrast for ease of use under the microscope. Before this can be done, the wax needs to be removed from the section so that the stain can eventually permeate all the sample areas. This is done by reversing the infiltration and dehydration processes before soaking in whichever particular stains that the pathologist or histologist would like to use, and which depends upon the type of tissue sample and what the scientist is looking for. In the case of collagen, Van Gieson stain is generally used – this stains collagen deep red [19][20].

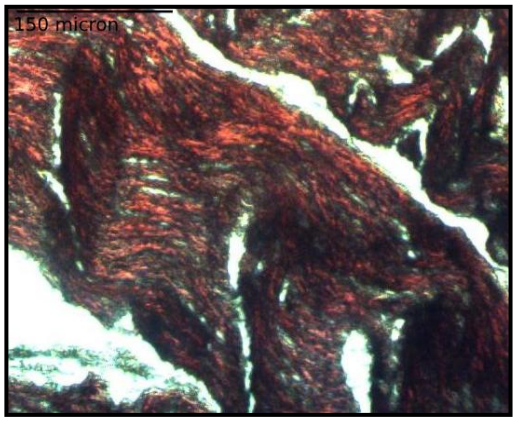

Fig 20
Microscope image of the 5 micron thick histological section – the collagen fibrils having been stained a deep-red by the Van Gieson stain.

Buffer preparation for use in liquid imaging

When imaging in liquid, the long-range electrostatic forces between the sample and the tip can be amplified by the solution in which the sample is being imaged, resulting in an interaction curve that has an ambiguous shape (figure 21) [13][14].

On inspection of the force curve taken in liquid it became apparent that the tip was experiencing very long range repulsive forces; the force curve did not show the typical sharp lines related to the attractive and repulsive regimes during extension and retraction, but instead a smooth curve, meaning that the force gradient in the repulsive regime was no longer proportional to the tip-sample separation. This sort of relationship gives ambiguous images [13][14].

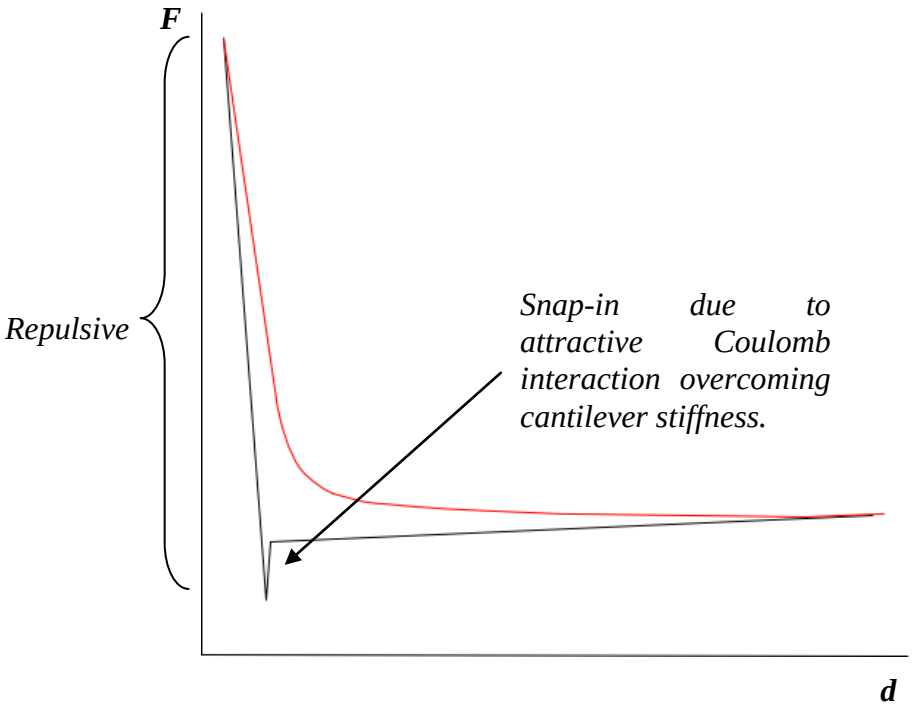

Fig 21
Illustration of the two approach force curves. The red curve shows long-range repulsive electrostatic interactions due to its curved nature, which can be compared to a standard Coulomb-interaction curve [5]. The black curve is of the form desired in this instance – an approximately proportional relationship is observed in the repulsive region, indicated.

To screen these long distance forces so that the force curve would revert to the desired shape, the buffer solution was changed from pure PBS (phosphor buffered saline), which has a pH of ~7.3, to a mixture of PBS and KCl (potassium chloride), to give a pH of 7.14 (±?).

Molar mass of KCl (FW) = 74.56 g/L
= 74.56 mg/mL
For 100mL of solution → 74.56 x 100 = 7456 mg/mL *gives* 1M

For 150mM (the amount needed for this solution) → 7456 x $150x10^{-3}$ = 1.1184 g

This amount of KCl salt was added to 100mL of PBS solution and allowed to dissolve. The pH of the solution was checked and found to be 7.14, before it was used in imaging. The force curves observed when using this buffer solution exhibited a higher level of proportionality in the repulsive regime.

Sample preparation at Diamond Synchrotron Source – liquid sample cells

The samples prepared for the x-ray diffraction experiments were to be as highly aligned so that the images were resolvable and in as natural conditions as possible. The beam used was also not very powerful (8.5keV) and so neither the substrate nor the sample could be very thick, as the beam would be too highly attenuated.

The samples used previously were prepared in much the same way as the aligned samples that I prepared for AFM imaging; the fibrils were placed on a kapton (appendix 4) substrate, the fibril bundle was separated and the fibrils themselves were

pulled into alignment using surgical tweezers. The kapton substrate was highly hydrophobic and so the collagen fibrils would generally start to "lift off" and become unattached from the substrate, especially when thicker samples were used. To stop this from happening, another sheet of kapton would be "sandwiched" on top of the sample. These samples gave quite adequate diffraction patterns that have been used successfully in the past and the resultant diffraction patterns gained during this experimentation time when using this preparation method were of similar quality [2].

Liquid sample cells were also available for use for the first time during this beamtime. The use of liquid cells would keep the collagen in a more native state, i.e. wet, and was predicted to minimise radiation damage to the sample by improving heat dissipation. The samples that could be used with this cell were also more diverse as there was no problem with "lift off" – for example it opened up the possibility of using whole (but very small) areas of tendon from the tip. This meant the natural structure of the fibril bundles was maintained

The first sample holder available was used originally for beam calibration using a medium-sized piece of rat-tail tendon.

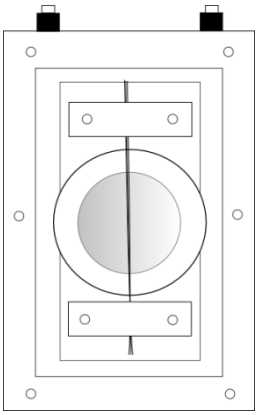

Fig 22
This diagram shows the inside of the cell body, where the PBS solution and rat tail sample would reside.

This cell was generally used with a much more intense beam than was being used in this experiment and so unfortunately the volume of liquid contained within the cell attenuated the beam too much and this cell was unusable.

A second slimmer cell was suitable for our uses. It comprised of a brass body with a window for a mica slide and a space for a washer, second mica slide and brass frame (see figure 23)[1]

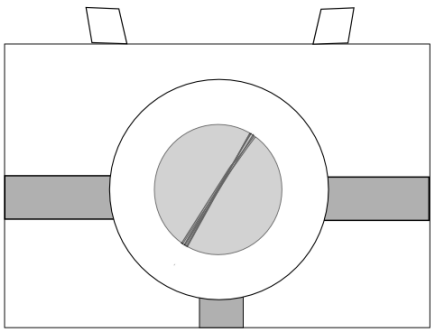

Fig 23
This diagram shows the front view of the sample holder, with the sample visible through the mica window

[1] Diagrams drawn personally after observation at Diamond Light Source [21]

The section of rat-tail was placed between the first mica slide and the washer and the space between was filled with PBS before placing the second mica slide over the top. A brass frame was then screwed into place over the ensemble.

The diffraction images that were taken using the samples in the liquid cells were far clearer that those found previously, due to the heat dissipation and the ability to use a very highly aligned sample. After this experiment it became clear that AFM images taken in wet conditions were necessary for use with the algorithm, as the dimensions and the shape of collagen fibrils are known to change in a hydrated environment [12].

X-ray Diffraction (at Diamond Light Source)

The diffraction images of the collagen fibril bundles were taken using the I22 undulator beamline at the Diamond Light Source on the Harwell Science and Innovation Campus in Didcot [21].

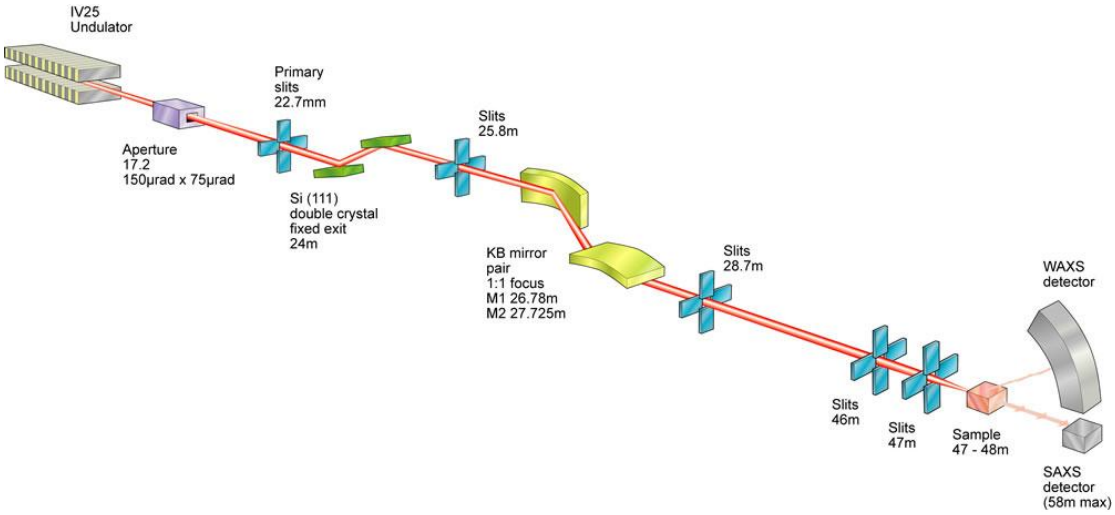

Fig 24
Schematic showing the I22 beamline set-up. The WAXS and SAXS detectors were not used, but a separate CCD camera was used as a detector [21].
The small angle source was suitable for use with the soft tissue samples that were being imaged and the use of a coherent beam meant that the "speckles" due to individual rows of fibrils in the sample were able to be resolved [2].

Beamline specifications	
Energy range	3.7-20 keV
D-spacing (not banding length) range	1-5000Å
Photon beamsize at sample	320 (H) x 70 (V) μm 2.7 (H) x 0.9 (V) μm (with micro-focusing) 50 (H) x 20 (V) μrad
Beam divergence at 12keV	0.6 x 0.7 mrad (with micro-focusing)
Source specifications	
Insertion device	In-vacuum U25 undulator
Nominal magnet length	2m
Nominal magnet gap	7mm
Magnet period	25mm
Aperture	150 μrad x 75 μrad
Optics	
Primary slits Si (111) double crystal monochromator Kirkpatrick-Baez mirrors	
Experimental Hutch and Sample Volume	
Flux @ 1 from source (ph/s)	10^{14} in 150 x 75 μrad
Sample distance from source	47-48m
CCD Detector to sample distance	5.255m

Table 1 [21]

The use of these particular monochromators allowed an energy of 8.5keV to be selected, the beam was also able to be cut down to a single coherence length - 30μm^2 – which is necessary for a correct ptychography approach [18].

Results and Observations

X-ray diffraction images

In the diffraction imaging of the collagen fibril bundles, the aim was to be able to resolve individual rows of fibrils so that the structure of the bundle could be solved after the phase had been found [2]. To do this, highly aligned samples and a coherent beam were needed. The images below express the characteristic diffraction pattern with an arc corresponding to the D-banding either side of the central beamstop [2][6][7]. The angular distribution between the arc edges (taking the centre of the beamstop as an origin) corresponds to the angular distribution of the fibrils. In the case of a completely disordered sample, the arcs would essentially form a circle around the central point. Individual speckles would be increasingly hard to resolve due to the fact that aligned fibrils are not amplifying the signal reflected from each individual fibril [6][7].

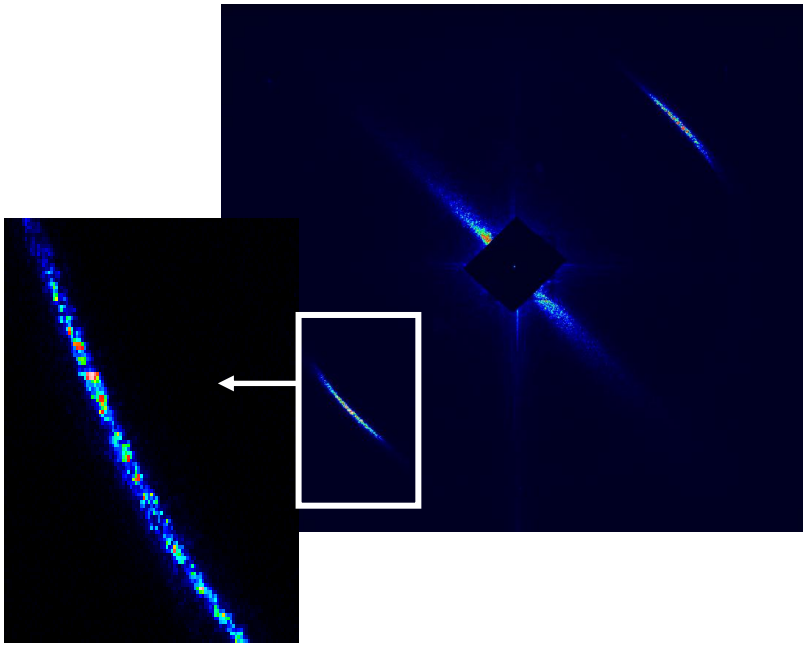

Fig 25
Dry aligned sample imaged in kapton "sandwich".
This image shows the characteristic diffraction pattern for an aligned collagen sample. Inset is a magnification of one of the arcs. The "speckles" observed correspond to individual rows of fibrils. These speckles can only be resolved using a coherent beam [2][3].

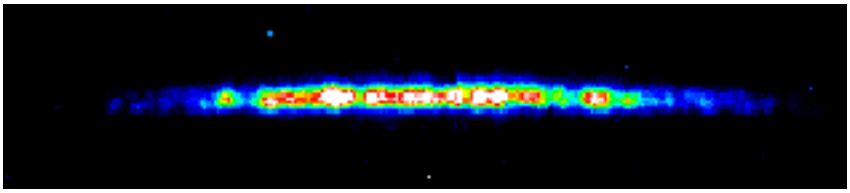

Fig 26
This shows a magnification of one of the arcs from a diffraction pattern taken of one of the samples in a liquid cell. It can be noted that the angular distribution of the fibrils is smaller and the speckles are brighter. This is due to the use of a more native sample and the more effective heat-dissipation, which slowed sample degradation.

The resultant D-banding lengths were found to be 64nm in dry conditions and 66.8nm in liquid. These figures correspond well to past results showing that the D-banding length increases in wet conditions [12].

AFM imaging

The height images in this report are generally represented using the amplitude or vertical deflection signals, as they will generally give a clearer picture of the fibril dimensions and characteristics than the true height signal. The height signal was always used when characterising the sample and when investigating its characteristic features to a higher degree, as it is this signal that gives information in the z-direction about the sample. The phase images are also used to some degree when discussing the interaction between the tip and the sample surface.

Imaging a single fibril

The first images taken were of a single fibril, found on the smeared samples. This was done so that the general fibril dimensions and the characteristic D-banding length could be investigated as well as to make the first inquiries into the effect of the AFM tip on the resultant image. The images produced were also used as a basic model for a collagen fibril in the development of the three dimensional ptychography algorithm. This model was then repeated in the x,y plane to give a plane filled with adjacent, aligned fibrils. This plane was then repeated in the z-plane in varying positions with respect to one another to give sheets of aligned fibrils, so that a three dimensional idealised model could be produced for comparative purposes with those images produced during x-ray diffraction [3].

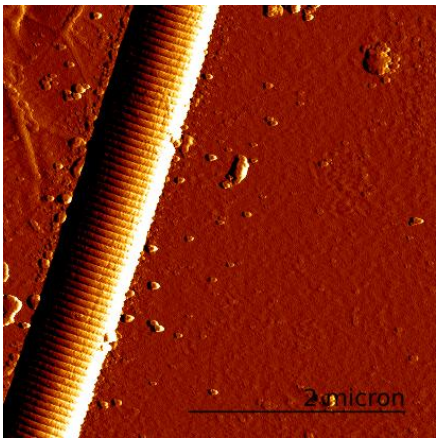

Fig 27
Amplitude image

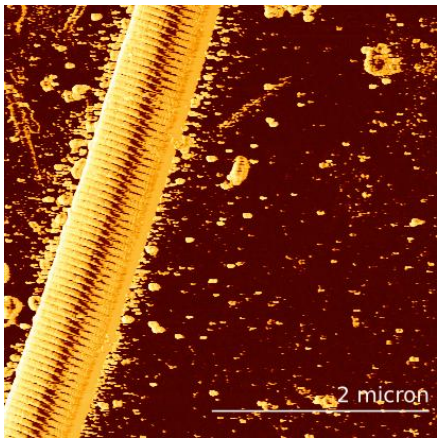

Fig 28
Phase image

The images were taken using a MikroMasch NSC15/Cr-Au BS tip (appendix 2). The phase image shows a darker region along the spine of the fibril, which would seem to correspond to a highly elastic area. After comparison with later images, as well as observing the three dimensional shape of the fibril (see fig 29 below) it would seem that this effect is in fact due to a variation in tip-sample interaction area [13]. This observation is important in the correct analysis of the fibril's mechanical features

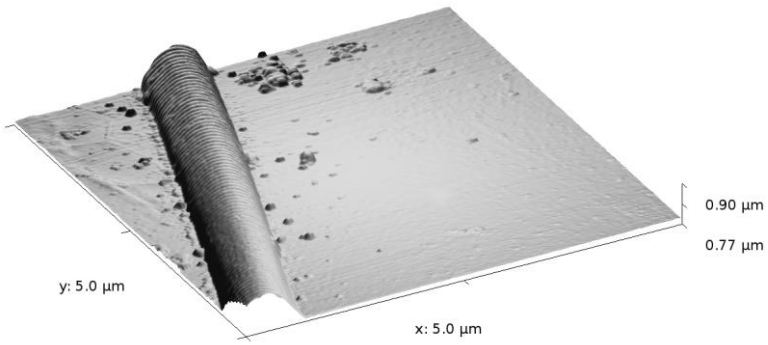

Fig 29
Three-dimensional image constructed using *Gwyddion* software [22]
Both the cross-sectional image (figure 30) and the 3-dimensional image above show the rounded nature of the fibril, which illustrates how the tip-sample interaction area will vary as the tip is scanned along the x-axis.

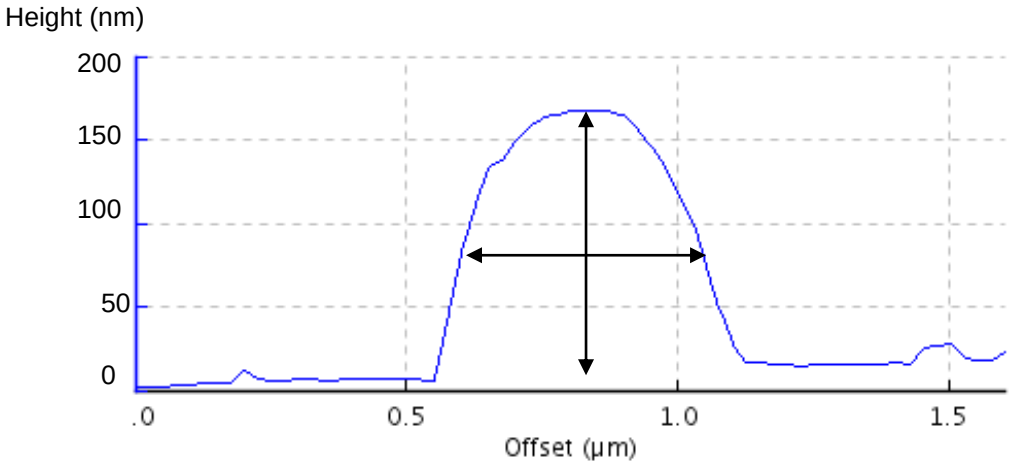

Fig 30
Fibril cross-section showing width and height measurements. The width of the fibril was taken at half its height.

After rescaling the x and the y-axes for the height image, it became clear that the cross-sectional profile of the collagen fibril takes on an elliptical shape. This "squashed" shape appears when the collagen is deposited on a substrate – in its native conditions the fibrils' cross-sections will be circular [12]. To find the original diameter of the fibrils, the heights and widths of a number of fibrils from various images were taken using the method described above, the cross-sectional area was found and the standard equation for the area of a circle was rearranged to give the radius.

Profile	width (nm)	height (nm)	cross-sectional area (m^2)	original diameter (nm)
1	285	87	1.94E-14	157.3
2	278	133	2.89E-14	191.9
3	398	161	5.03E-14	253.1
4	319	115	2.89E-14	191.8
5	363	139	3.97E-14	224.9
1	218	174	2.97E-14	194.5
2	212	137	2.28E-14	170.3
3	144	101	1.14E-14	120.4
4	157	115	1.42E-14	134.7
5	196	120	1.84E-14	152.9

Table 2

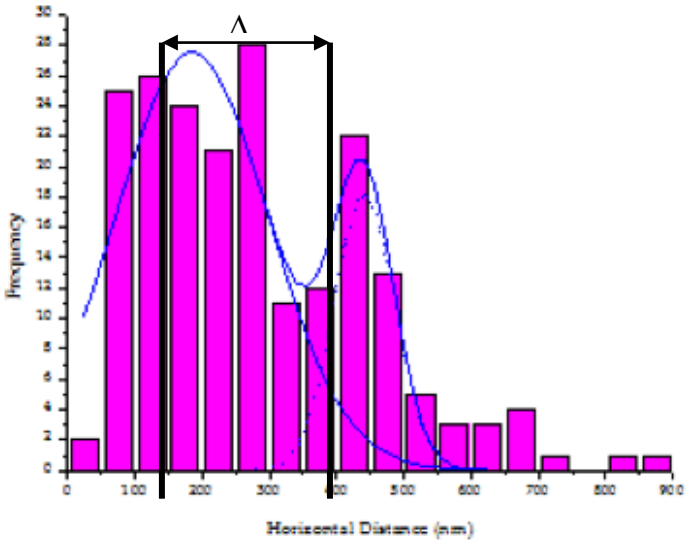

Fig 31
Histogram illustrating the normal distribution of rat-tail fibril widths when imaged in air [23]. The fibrils imaged here fall in the range indicated by Δ.

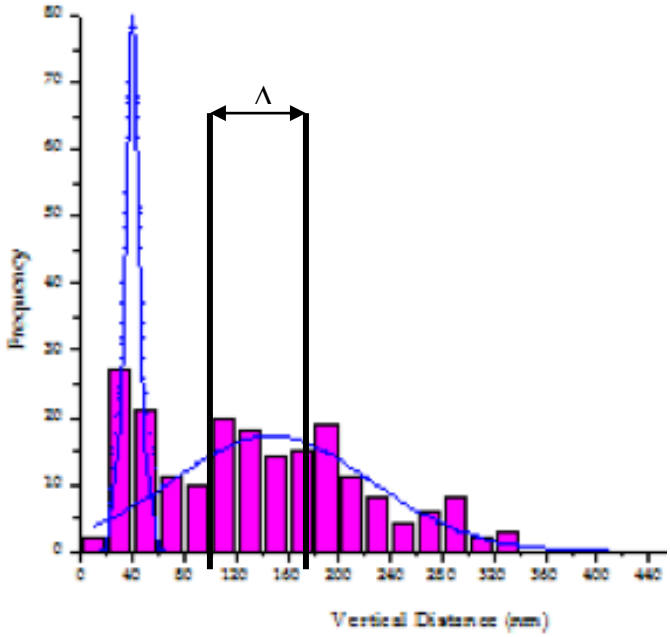

Fig 32
Histogram illustrating the normal distribution of fibril heights when imaged in air [23]. Once again the fibrils here fall into the range approximately indicated by Δ.

By knowing that the dimensions of the fibrils imaged here fall within the normal distribution implies that the measurement is reliable. The range within which they fall also implies that they are mature fibrils [12].

The shape and dimensions of the D-banding were probed next, to compare with results that have been published in the past so as to see if the results shown here were reliable as well as to investigate the effect of the tip-shape on the profiles reported. The shape and size of the tip compared to the dimensions of the banding troughs was also investigated; this comparison was done so as to find out if the features shown were in fact a convolution of the tip shape and the feature itself.

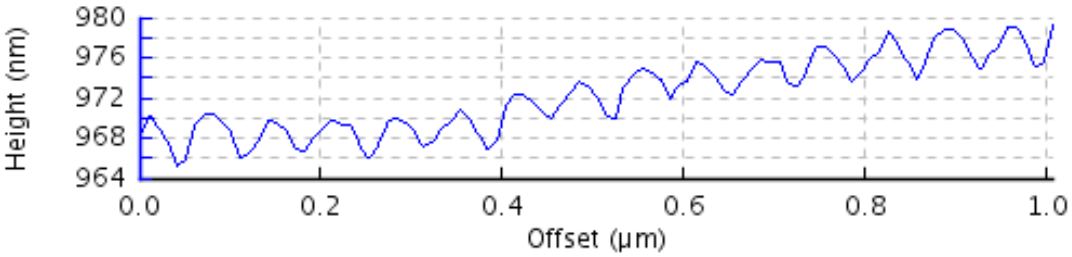

Fig 33
Cross-section of fibril D-banding with a height showing the source of the cross-section. Note the typically rounded shape of the bands.

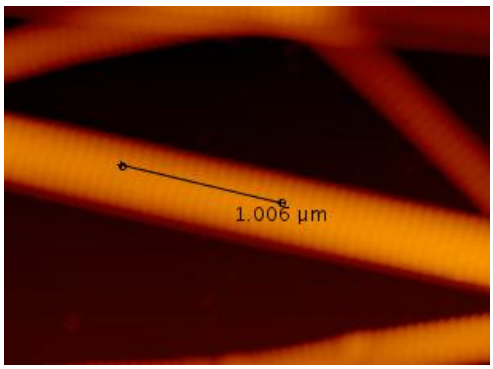

The depths of the D-banding, the peak-to-peak widths and the opening angles of their troughs were found so as to characterise them with respect to the dimensions of the tip being used. This should show whether the tip used was of the same dimensions as the troughs in the banding found here. If so, the tip-shape may be deeply influencing the banding shape reported.

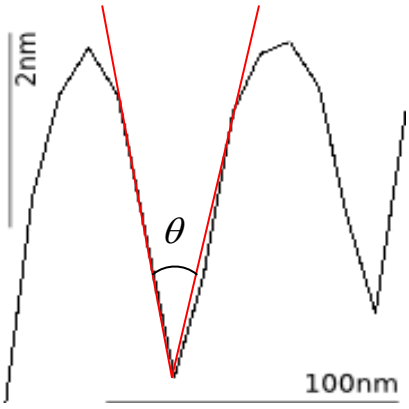

Fig 34
Illustration of the opening angle of the bands shown on a section taken from the profile in figure 33.
The trough depth and peak-to-peak distances were rescaled before θ was found

trough	peak-to-peak width (nm)	depth (nm)	theta (º)
1	39.9	3.15	81.03
2	41.8	3.36	80.87
3	41.8	3.36	80.87
4	43.7	2.63	83.15
5	43.7	2.94	82.34
6	38.0	2.52	82.44
7	57.0	3.36	83.28
8	45.6	2.84	82.91
9	53.2	3.36	82.80
10	45.6	2.63	83.43
11	55.1	3.26	83.26
12	43.7	2.63	83.15
13	34.2	3.05	79.90
mean	44.9	3.00	82.26
standard deviation	6.7	0.33	1.18

Table 3

The tip was then imaged using "TipCheck" [17][22] and a profile was taken across its two major axes to find its radius and the angle at its apex.

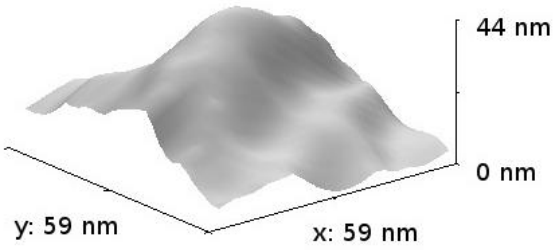

Fig 35
3D image of the tip apex. The tip appears to have taken on a flattened shape that's quite narrow in one direction but very wide in the other – this will affect the images produced.

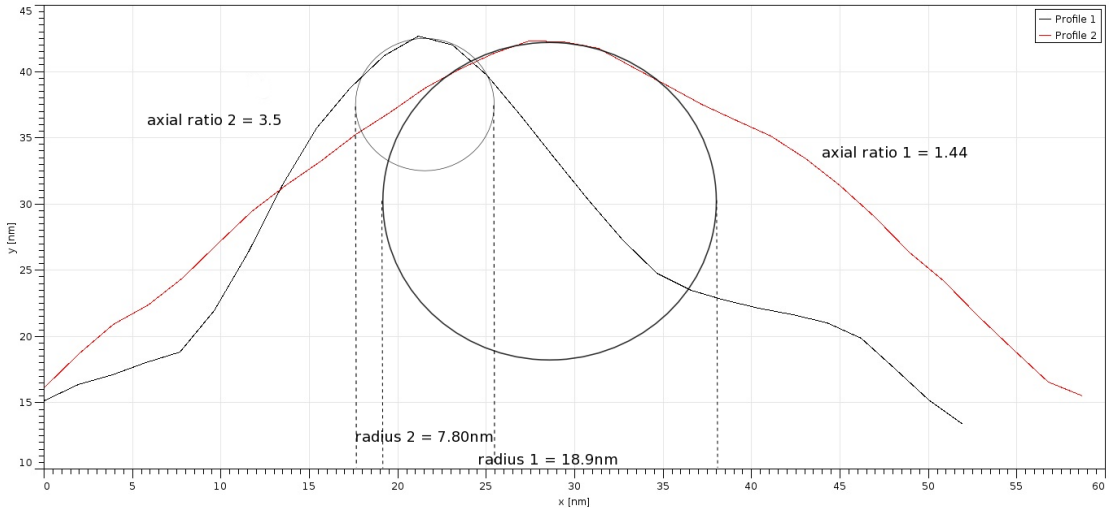

Fig 36
Profiles of the two major tip-axes. Circles have been fitted to the profile to find the tip-radii, which were found to be 18.9nm in one direction and 7.80nm in the other. The angle found for the larger part was 118º, 87º for the smaller profile.

The peak-to-peak widths of the D-banding troughs were approximately twice the size of the larger radius, and the trough depth was significantly smaller than the larger radius. Therefore the banding shape is clearly not a pure image of the tip apex, but the dimensions are of the same order, and the apex angle of the smaller tip-point is close to the average opening angle of the D-banding, meaning the convolution of the tip and the sample is non-negligible [13].

Imaging collagen matrices

Collagen matrices found on both the smeared samples and compressed collagen gel were imaged before the preparation method of keeping samples aligned was developed for correlation with the ptychography algorithm and also as a first investigation into how the fibrils are packed with respect to one another.

Amplitude image

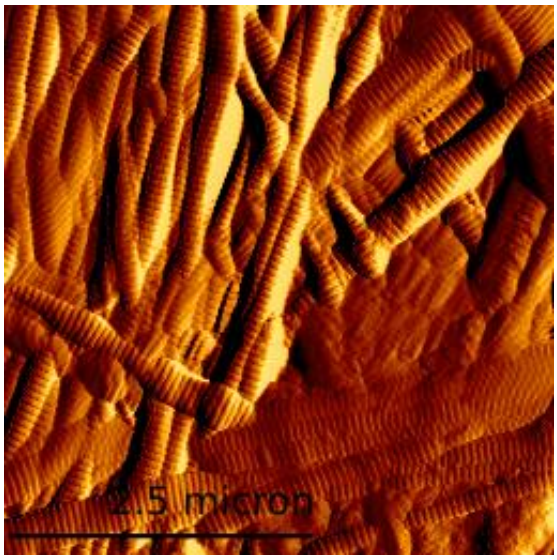

Fig 37
The sample shown in this figure is taken from one of the smeared collagen samples using a MikroMasch NSC15/Cr-Au BS tip (appendix 2).
The D-banding is still very clearly shown through most of the image, as are the fibril's shape and dimensions, but the natural alignment of the fibrils is almost completely unpreserved; the comparative models made from this will hence be less realistic with respect to the diffraction images.
Finer details are also not resolved due to the roughness of the sample – the topography is converted into a grayscale with each of the tones representing a height range; if there is a large range of heights in the image as a whole, the range per grayscale tone will also be larger [13][14].

Amplitude image

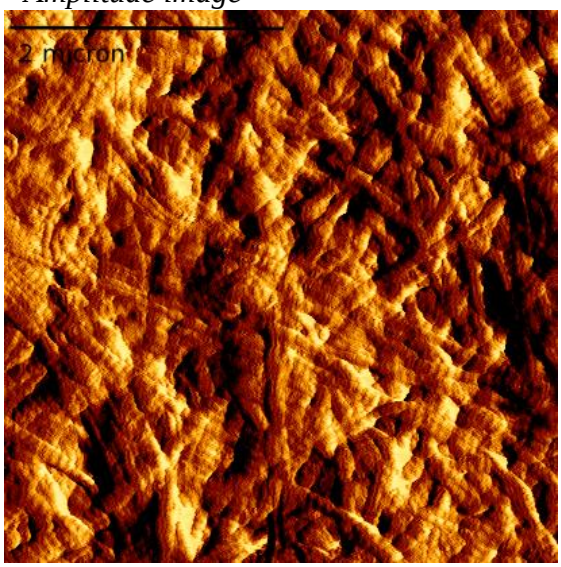

Fig 38
The sample shown above is taken from a compressed collagen gel made from reconstituted rat-tail collagen. The formation of the fibrils is much like that found in skin and cartilage. Again the tip used was a MikroMasch NSC15/Cr-Au BS tip.
There is no alignment preserved in this sample, meaning that the images gained are useless with respect to the development of the current ptychography algorithm. The finer details of the fibril structure are also less well-resolved than those on the smeared sample image due to a further increase of sample-surface roughness.

The images previously used for the comparative model in the development of the ptychography algorithm were very similar to those shown in figure 37, above. Although quite realistic models could be developed using these images, they did not preserve the natural alignment of the rat-tail tendon and were hence not the most suitable images for this use [2].

Aligned samples

The next samples imaged were first and foremost for use in the development of the ptychography algorithm. They were taken from the aligned samples that had been hand prepared. A variation in D-banding shape was observed and the relationship between phase images and height images was further investigated.

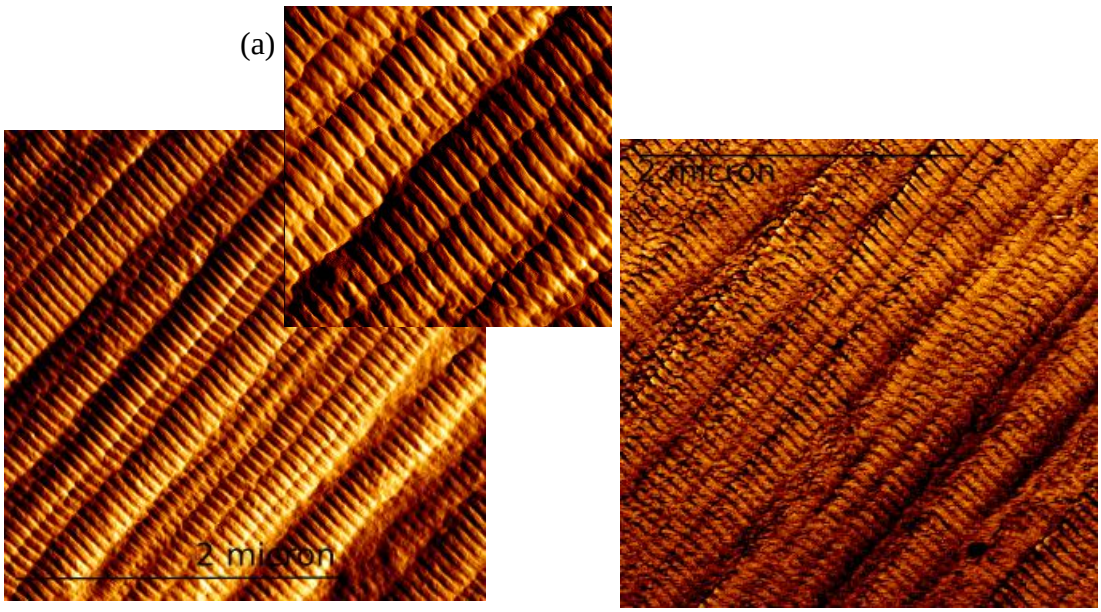

Fig 39
Images taken using a MikroMaschNSC15/Cr-Au BS tip - new.
These images show a far higher level of alignment to those taken previously, making them far more suitable for use in the development of the ptychography algorithm. The feature edges are also much more defined and in the amplitude image a variation on the banding shape can start to be observed (as shown to a higher degree in fig (a), which was taken at higher resolution).

The images here also exhibit signs of a double-tip effect

The more prominent ordering of the collagen fibrils also makes the comparison between the phase and amplitude images far easier. It is observed that the fibril features seem to correspond in the two images types, which prompts the question whether the contrast in the phase image is due to the topographical features of the sample-surface, or whether there is a variation in viscoelastic properties that corresponds to different areas in the D-banding.

By using the novel preparation method described in the materials and methods section to prepare samples that retained areas of natural alignment, images were produced that were not only clear and could be analysed with respect to the superficial structure, but also will be the closest in conformation to those prepared for the x-ray diffraction imaging; this will give a more realistic comparison ptychography algorithm [3][12].

By imaging a sample with a low degree of roughness using a new (and hence sharper) tip and an optimum scan angle the overall quality of the images was ameliorated, resulting in the observation of squarer D-banding and small-scale features in the banding.

Measuring the D-banding length

The average D-banding length was found by taking profiles of the fibrils (of the type shown in figure 33) parallel to their length from various height images to compare to accepted values. The lengths of these sections were found and divided by the number of bands present.

Profile	L (μm)	Bands	L (nm)
1	1.373	21	65.4
2	1.340	20	67.0
3	0.258	4	64.7
4	0.782	12	65.1
5	0.686	11	62.3
6	0.631	10	63.1
7	0.635	10	63.5
8	1.570	24	65.4
9	0.845	13	65.0
10	0.612	9	68.0
11	0.678	10	67.8
12	0.340	5	68.0
Mean			65.5
Standard deviation			1.9

Table 4

The mean value of the D-banding length was hence found to be 65.5nm ± 1.9nm.

A second approach was taken to find this length that used fast fourier transforms from a number of images to find the average D-banding length. This approach was also used in a number of ways to further characterise the sample

Characterisation of samples and images using fast fourier transforms (FFT)

The images taken of the hand-aligned samples were then characterised using a fast fourier transform process on the image analysis software *Gwyddion* [22]. This characterisation method was used so that the average D-banding could be easily found and to see if the images were suitable for comparison to the diffraction images in the development of the ptychography algorithm; the comparative images need to have a fibrillar angular distribution of <10º, the characteristic bands due to the D-banding of the fibrils need to be bright and there needs to be some modulation present in these bands – the aforementioned "speckles" [2][3].

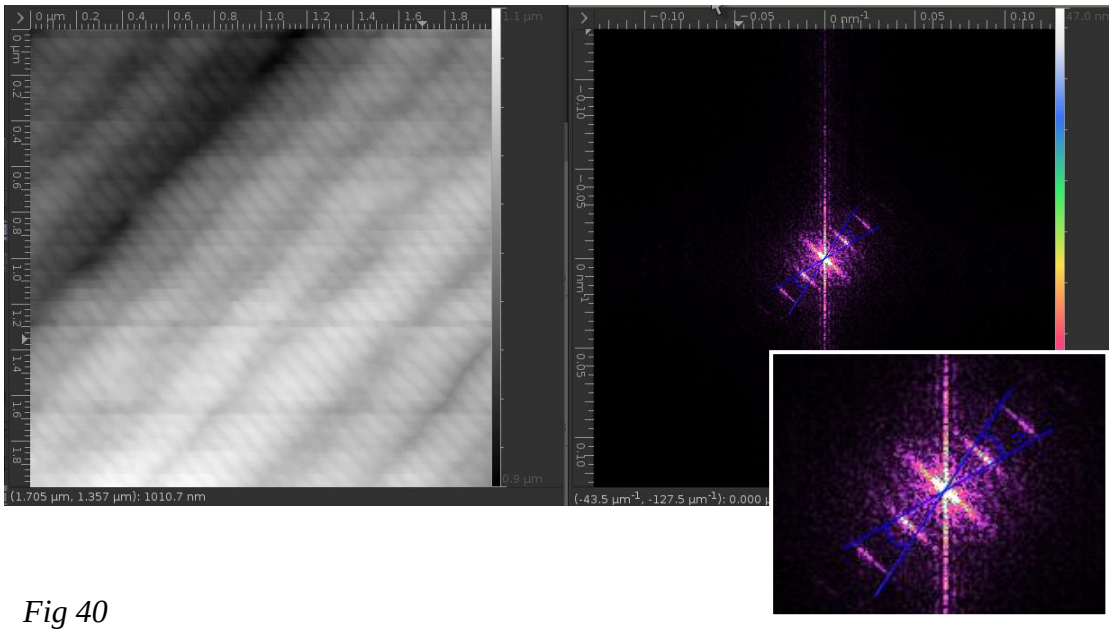

Fig 40
This image is a screen dump taken from the *Gwyddion* software [22]. On the left-hand side the height image that had the FFT performed on it is shown, and on the right hand side the resultant transformation is shown. The symmetric banding either side of the central region is due to the D-banding on the collagen fibrils, the average length of which was found to be 65.2 nm ± 4.0 nm, found from a range of images. The inset image is a close-up of the banding, showing how the angular distribution was found as well as showing the "speckling" in the band.

It is observable that these FFT images show the same characteristic arcs either side of the central point as were observed in the real diffraction images [3][6][7]. They also show secondary bands that again correspond to the D-banding, but were not visible on the diffraction images as the detector was not large enough to capture them. The distance between first and second bands corresponds to another D-banding length. These similarities show that the AFM images were suitable for use in the ptychography algorithm

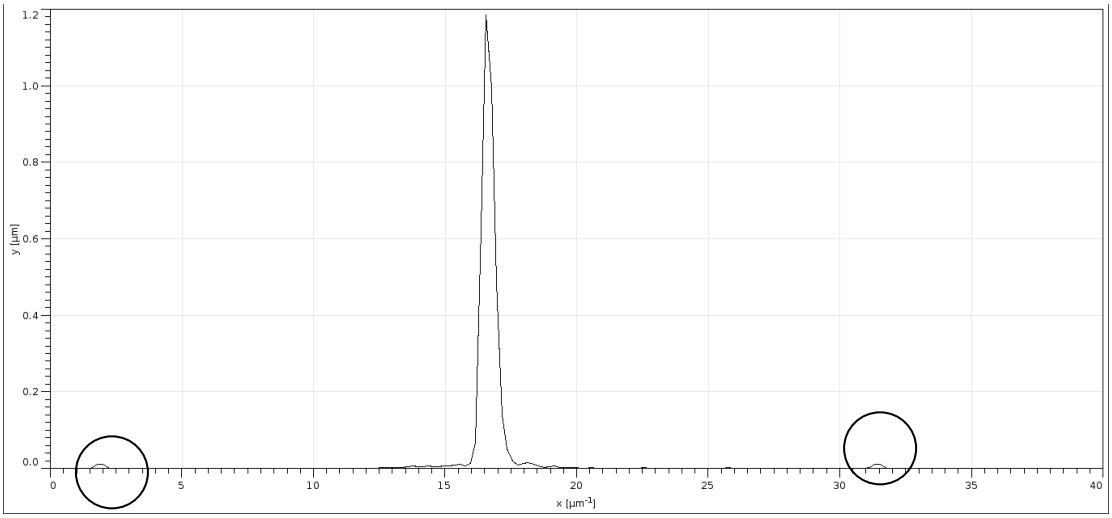

Fig 41

The error on the D-banding found using the FFT was taken by finding the banding width on the FFT using the profile tool on the *Gwyddion* software. The circles on the diagram highlight the peaks due to the banding – the distance between the inner edges and the outer edges of the two peaks was found before transforming them into real-space distances, and subtracting the values from one another. This was done with a range of FFTs to find the final error-value.

The values found for the D-banding using the two methods were within an error value of one another, and so both can be said to be reliable. The values found are within the normal range for the D-banding length of collagen, which is between 64 and 67nm, with tendon usually having a value of ~67nm in wet conditions [4]-[12].

Investigation into the shape of the D-banding

The shape of the collagen D-banding when imaged using AFM is often shown to be rounded in nature[8]-[11], a tendency also expressed in many of the images taken in this project. As the images taken improved in quality and resolution, however, a squarer banding was seen, which is in better agreement with the images of collagen taken using electron microscopy methods [10][24]. The fibril profiles taken from the height images also started to express smaller-scale details on the peaks, as illustrated inset in figure 42, below.

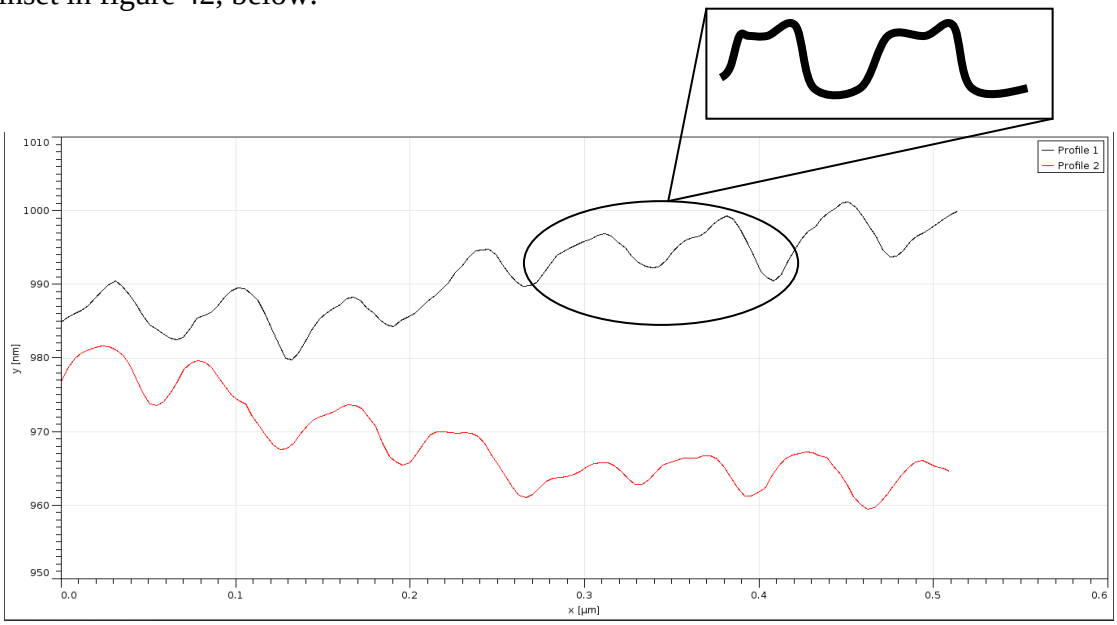

Fig 42
This image shows two profiles taken from the same image taken using the MikroMasch NSC15/Cr-Au BS tips. The shape of the D-banding shows indications of smaller scale structure. The troughs of the banding are still quite rounded in comparison to many of the peaks. The rounded trough bases may in fact be a convolution of the tip-shape and D-banding shape rather than a real feature [13]. Highlighted are two banding peaks that show observable smaller-scale structure.

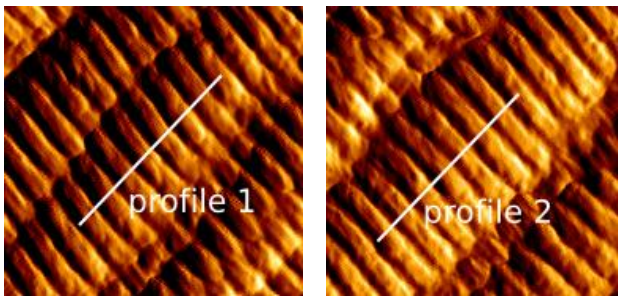

Fig 43
Shows the profiles from figure 42 as they were taken from the original image.

The lengths of the troughs were measured using the same profiling method as described previously to gather if the distances would correspond to the gap region in the collagen molecular packing model (see figures 2, 4) [8][11].

The trough widths were found by taking the full width, half maximum (FWHM) of the troughs.

Trough	FWHM (nm)
1	39.4
2	24.7
3	20.9
4	28.5
5	30.2
6	25.7
7	34.6
8	30.1
mean	29.3
standard deviation	5.8

Table 5

In the quarter-staggered packing model, the gap region is hypothesised to be 0.4D = 0.4 x 64 nm = 25.6nm, taking the average D-banding length found earlier. This is within the error of the trough-width found here.

This finding relates well to the standard assumption that the trough areas relate to the "gap" region in the axial model (see figures 2,4) [8][11].

After comparison with related structures such as Ultra Long Spacing fibrillar collagen imaged using AFM as well as EM images of fibrillar collagen, and taking into account how much the banding was affected by the blunt tip shown earlier, it seems highly likely that the rounded shape of the banding troughs is due to a tip-sample convolution rather than a real feature. When comparing the images found here to those taken of ultra long spacing fibrillar collagen, the peak shape is observed to be similar, but the trough is far flatter [25]26]. The peak in these images, however, is comparable to the known shape of a convolution between a conical tip and rectangular obstacle, as illustrated in figure 15 in the introduction. This begs the question whether the peaks shown in both my own images and the images provided by ULS fibrillar collagen AFM imaging is a reliable profile or whether it has been strongly affected by the tip-shape.

Fig 44
Profile of ULS fibrillar collagen, showing flat trough bases and curved peaks.

This hypothesis was further supported when looking at images whose surfaces were at an angle relative to the tip-axis (z-axis), illustrated in figure 45, below

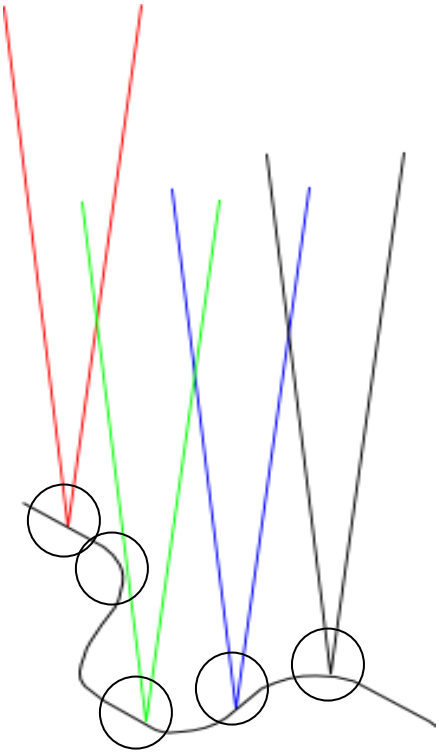

Fig 45
Idealised diagram of a tip interacting with a modulated, angled sample. The different coloured Vs represent the tip at different positions along the sample, with the circles highlighting interaction areas. It can be observed that the green tip has a significantly larger interaction area than the others.

The resulting banding profiles were interesting in that the banding peak edges were at different angles with respect to the trough base, with the elevated edge having a consistently wider angle (see figure 46).

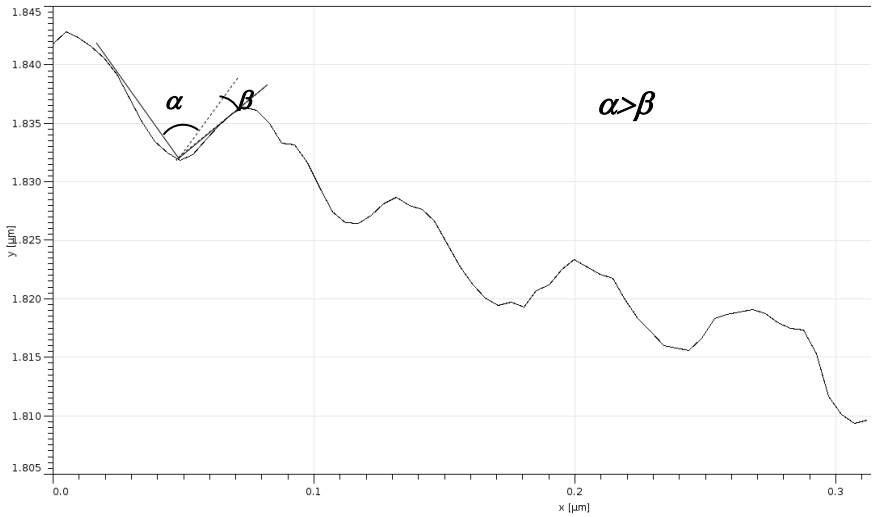

Fig 46
Profile of a fibril along the D-banding where the sample surface was not parallel to the x-axis.

The variation in peak walls with surface-angle and the observation that the lower peak-wall is approaching perpendicular with the trough-base is best explained by convolution effects.

Finer D-banding features

There has been some precedent in published work for small-scale features on the D-banding, particularly in electron microscopy images. Densitometric traces of negatively stained type I collagen taken using electron microscopy have shown similar profiles to those observed in the profiles taken during this project, as illustrated in figure 47, below [27]. These traces reveal further banding between the two features on the banding peaks that have been observed in the profiles shown in traces such as figure 42 and figure 46. These features have been hypothesised to correspond to exposed amino acid side-chains along the length of the collagen molecule [6][7][8], these side-chains may be charged, as their appearance is quite often more prominent in positively stained samples, which would imply the presence of negatively charged side-chains. The densitometric traces also show a much squarer profile than those generally taken with AFM.

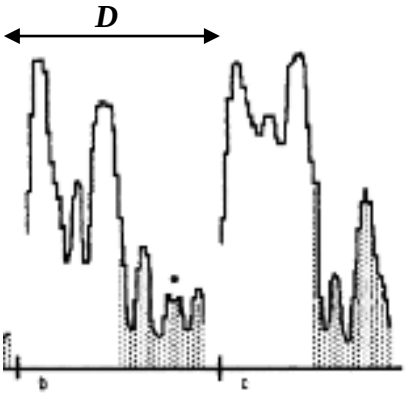

Fig 47
Two densitometric traces of type 1 collagen banding taken from [14]. The profiles show a squarer D-banding along with similar sub-structural details as those shown in both height and phase images (fig 49).

High resolution AFM images taken of collagen microribbons formed in vitro have also been found to exhibit the same small-scale features [8]. These microribbons exhibit a thickness of ~3nm, which is the thickness of a single microfibril, in the order of a collagen molecular width. The matrix was grown so that the collagen microfibrils covered the substrate surface with a homogeneous layer, this is unlike native type I collagen taken from tendon, in that it hasn't formed larger individual fibrils [8]. The images taken with high resolution AFM still seem to shown an overall curve to the envelope of the D-banding

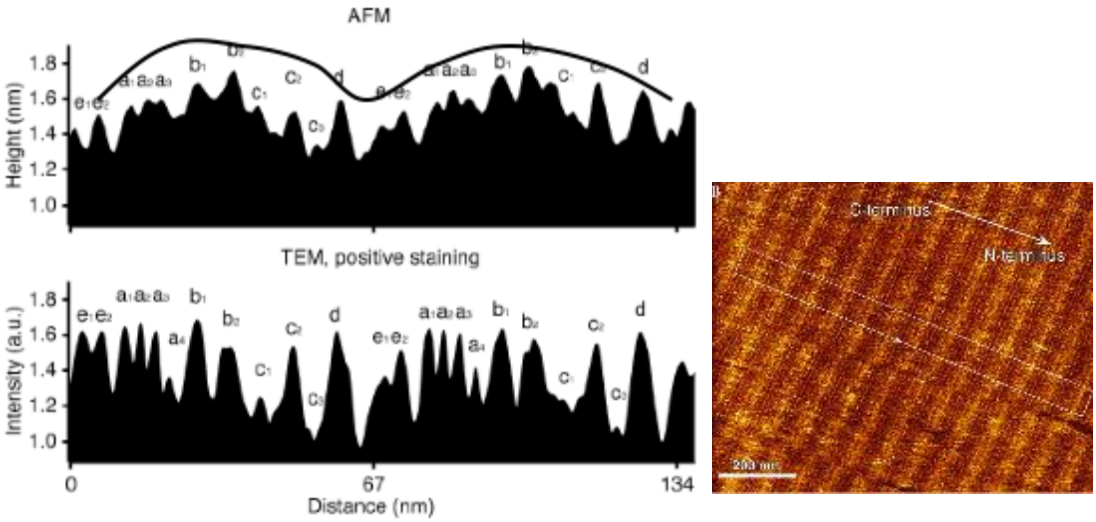

Fig 48

Banding profile taken from [8], with the curved outline added later. 97 % Type I collagen, 3% type III microribbons grown in vitro, derived from bovine dermal collagen. Imaging was performed in liquid using intermittent contact mode. The AFM profile was found by taking an average of the height profiles of a 980 x 70 nm^2 area. Imaging was taken in a buffer solution of pH 9.2.

The image on the right shows the area that the profiles were taken from.

It would be very hard to argue that the overall rounded shape to these bands is due to a convolution of the surface features and the tip shape, as the tip has been able to resolve far smaller peaks. It has een hypothesised that these bands may be due to exposed, charged amino acids (as mentioned previously), so that the peaks may not be purely topographical features, but due instead to long-ranging electrostatic interactions 81]. This effect could also alter the overall apparent D-banding envelope shape, and make it appear more curved. However, this imaging was performed in a buffer solution with a high electrolyte concentration, which should screen these charges, resulting in purely topographical features [8][13].

The nature of this sample is very different to the samples used in this project. The ribbons were grown in vitro and have a thickness in the order of one or two molecular widths, whereas native rat-tail fibrils are approximately 100 x this size. Because of this, the sub-fibrillar packing model may be different and the characteristics may change as the structure size increases. These differences may result in a far squarer D-banding for native fibrils as well as screening of the finer banding details. The microribbons were also imaged in liquid, which may also change the banding shape, resulting in an overall rounded envelope [8].

It would be interesting to further investigate the banding shape and small-scale features in liquid and to compare the results to images such as these to investigate how the banding shape changes in liquid.

Phase-topography comparison

After investigating this variation in D-banding shape, the relationship between the phase signal and height signal was investigated to see if there was any relationship between the viscoelastic properties of the sample and the D-banding area. This was done by overlaying profiles taken from corresponding areas on a phase image and a height image from the same sample. This was also done so as to further investigate the smaller-scale details of the banding shape, as the phase signal is very sensitive to topographical changes as well and may reveal finer details within the banding[13][14][15].

Due to the sensitivity of the phase signal to both the viscoelastic properties of the sample and the variation in topography, it is very hard to analyse the signal simply in terms of either one contribution [13][14][15]. This is especially prominent in this case as the peaks and troughs of the banding correspond quite so well, as illustrated in figure 49, below.

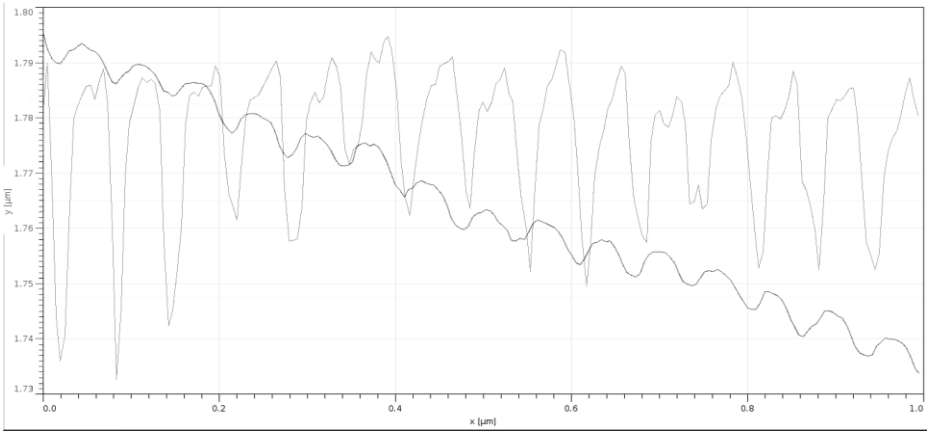

Fig 49
The profiles shown above were taken from an image that had used a sharp (new) MikroMasch NSC15/Cr_Au BS tip. The paler grey line corresponds to the phase signal and the darker grey curve corresponds to the height signal.
The peaks and troughs of the two signals are quite well correlated, which may relate to a higher elastic region in the banding troughs and a higher viscous region at the banding peaks, or the phase variation may simply be due to the features themselves.

It can be noted that the phase peaks (and some troughs) show sub-D-banding features

Histological section

The histological sections were imaged using both x-ray diffraction and AFM. Only the thickest of the sections showed any diffraction pattern when used in the x-ray experiments, and these were faint, had a large angular distribution with no noticeable speckles and a large degree of noise. Because of these factors they were neither suitable for use in the development of the ptychography algorithm nor for use in the general investigation of the native fibrillar packing of collagen at the current state of the project.

Height image

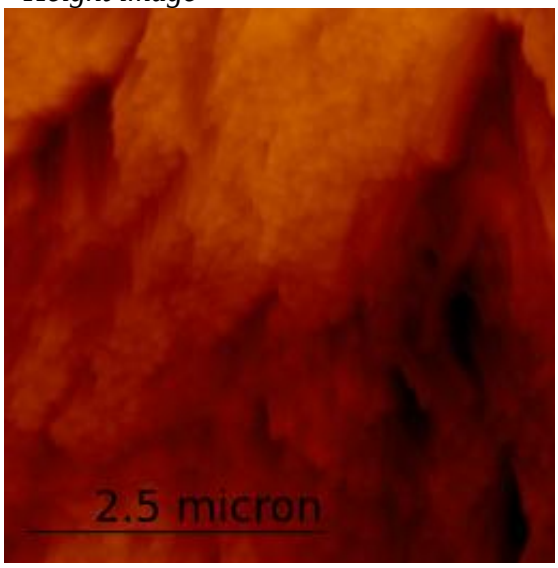

Fig 50
Image taken using a MikroMasch NSC15/Cr-Au BS tip - new.

The AFM images taken of the histological section show a large amount of fibril chopping along the surface of the sample, as illustrated in this image. The fibrils have retained a lot of their alignment, although not to the same degree shown by the images taken of the hand aligned samples. The presence of the chopped ends of the fibrils as well as some remnants of wax (observable in fig… below) made the samples unsuitable for use with x-ray diffraction imaging. These factors are also the reasons why the images will be unsuitable for use as comparative models for the ptychography algorithm development.

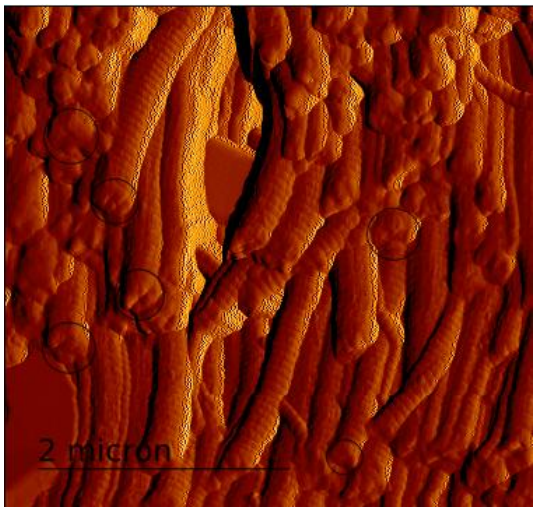

Amplitude image

Fig 51
This higher resolution image of the histological section shows the residual wax and also illustrates the extent to which the fibrils have been fattened – an effect that may be due to the picric acid present in the Van Gieson stain.

Several fibril ends that are available to the AFM tip across the entirety of their surface – these cross-sections would be suitable for force-volume measurements, giving further insight into the internal makeup and mechanics of the fibril [20].

Imaging in liquid

The images taken in liquid were imaged in contact mode, as intermittent contact mode proved problematic – the resonant frequency and phase curves of the tips could change midway through imaging and their were difficulties in identifying the point of contact between the tip and the sample. These difficulties were due to the fact that the surrounding liquid would also be driven into oscillation when the cantilever was.

There also were some problems in knowing the best area of the force-curve to be imaging in when using contact mode, but the best area was eventually found to be immediately after snap-in of the tip. The relationship between force and distance is approximately proportional in this region and the force incident on the sample is not so great as to drag the sample surface to a high degree.

The images taken were from the smeared samples as those samples with areas of natural alignment were quite thick and became much thicker after swelling due to liquid absorption [12] and as a result the sample would move quite a lot during imaging. This would result in unreliable images.

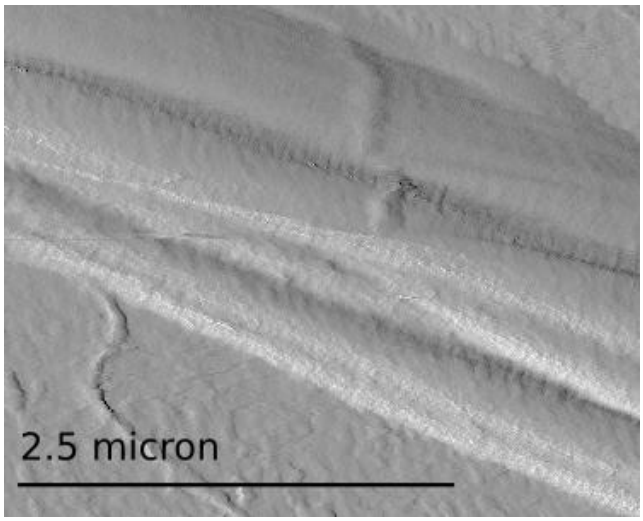

Fig 52
These images were taken using Veeco DNP tips (appendix 2).

The D-banding is far less obvious on this image compared to those taken earlier in dry conditions, with some areas not showing any banding at all. This is due to the swelling of the fibrils, which can be up to 100% [12].

The dimensions of several fibrils were taken to compare with those taken in air (*Table 2*).

Profile	Width (nm)	Height (nm)	Area (m^2)	Real diameter (nm)
1	172.50	224.25	3.04E-14	197.68
2	167.90	224.50	2.96E-14	194.15
3	174.80	220.80	3.03E-14	196.46
4	165.60	186.30	2.42E-14	176.65
5	158.70	196.65	2.45E-14	177.66

Table 6

The "real" diameters of the fibrils imaged here are of a size comparable to those imaged in air listed in table 1. By comparing this result to results published in the past, it can be hypothesised that the fibrils imaged here are less mature [12].

The value for the D-banding length was found using an FFT performed on the vertical deflection image, as the D-banding was almost invisible on the height images. The D-banding could not be found using the profiling technique used in previously in air as there was not enough contrast between the bands to count them accurately.

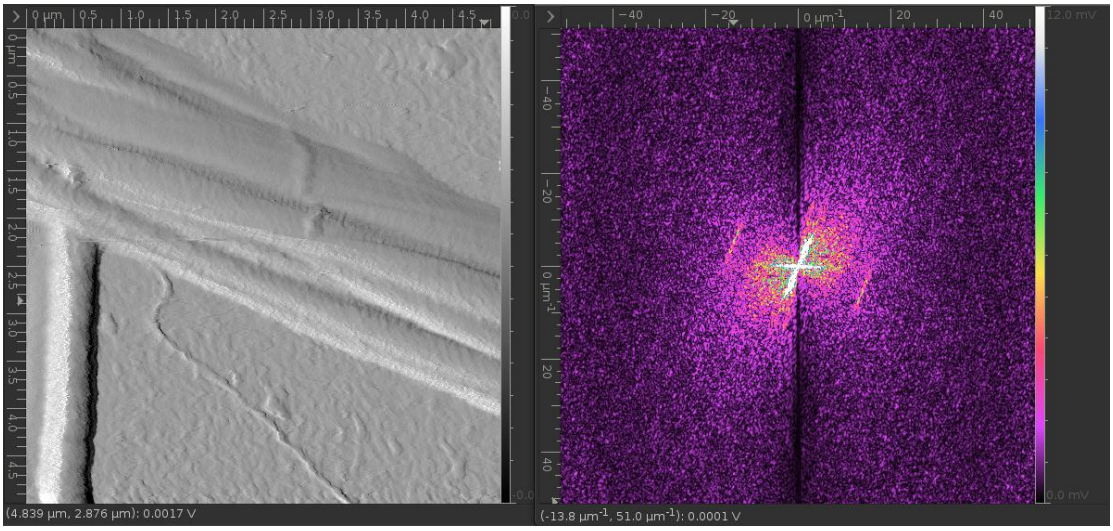

Fig 53
This image shows a screen-dump from the *Gwyddion* software illustrating the FFT taken of the vertical deflection image of the fibrils imaged in wet conditions. The characteristic features due to the D-banding are clearly seen in this image and the banding length and error was found in the same way as described in previously

The FFT image is far noisier than those taken of the height images as there are far more details present in this image – in the height image the smaller details on and around the fibrils are not so easily visible, as the vertical deflection image, like the amplitude image, highlights the feature edges. This results in greater contrast and therefore a larger number of features visible across the image [13][14].

Unfortunately, the aligned samples were less suitable for work in liquid, as they were quite thick in the areas where the natural alignment was well preserved and would swell up. This swelling resulted in movement of the sample and increased sample roughness; the z-range of the piezo also had to be extended to minimise tip and piezo damage, which meant that the images were of a lower resolution, as the piezo was less sensitive to smaller changes.

Another problem with the aligned areas when imaging in liquid is that they are laterally far from the glass substrate (see fig 54), as such there is no "control" to return to. If an experimenter knows what a glass surface looks like when imaged under the AFM, then it can be used comparatively if included in the scan region to check that the images of the fibrils gained are reliable. The worry in not having this control is that the tip may be scanning at a very large tip-sample separation – "floating" above its surface – which would result in a low-res image that doesn't give a complete picture of the surface features.

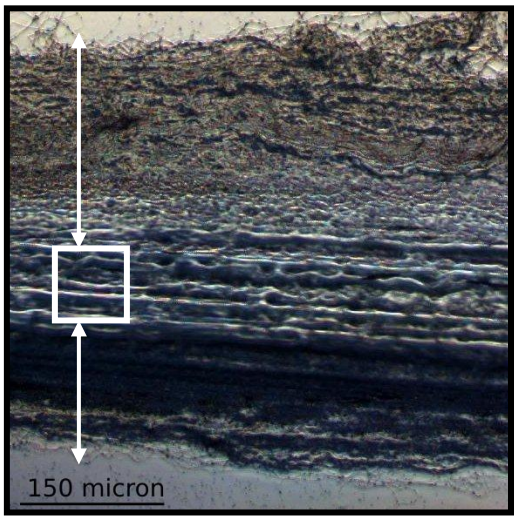

Fig 54
Illustrates the distance from the scan region to the glass substrate. This shows that it is impossible for the "control" to be reached while still imaging in an aligned area.

The problem of sample movement may be rectified by fixing the sample using aldehydes [19]. Unfortunately, this may change the fibrils' natural response to a liquid environment, resulting in images that would not correspond to the x-ray diffraction images taken in liquid cells. This technique may also ruin the changes of further investigation into how the D-banding and its smaller features change with a liquid environment.

The problem of a lack of "control" may also be solved now that the appearance of fibrils in liquid has been shown. If one knows what the fibrils should look like, the challenge is instead the acquisition of higher resolution images that would show sub-D-banding structure

The use of intermittent contact mode in liquid with a more alkaline solution, such as that used to image the microribbons [8] would also be a viable option, although once again this may require the use of aldehydes to fix the sample so that it doesn't move during imaging due to the sample thickness.

Summary and outlook

The sample preparation protocol has been greatly improved in both AFM imaging and x-ray diffraction imaging. The use of a novel preparation method that preserves areas of natural alignment in hand-prepared samples has resulted in clearer and more realistic images for use in the development of the ptychography algorithm. This method has also resulted in images of finer structural resolution due to a decreased level of surface roughness; this improved resolution has led to the observation of sub-D-banding structure. The use of liquid cells during diffraction imaging has resulted in clearer images in a more native environment, meaning that the three-dimensional structure, when it is eventually resolved, will be a more realistic representation of the collagen fibril bundles' native state.

The affect of the tip-shape and size on the images produced was investigated and found to have a significant effect on the shape of the D-banding reported as well as the resolution of finer banding features within the overall D-banding. This conclusion is important with respect to the use of the AFM images as a comparative model in the development of the ptychography algorithm, as the model for the iterative algorithm requires the modelling of a fibrillar profile. Knowing that the tip is sharp and has a regular shape at its apex is important in this respect to minimise convolution effects.

The observation of sub-D-banding features in the images taken relates well to images taken using electron microscopy [8], and although there are some discrepancies in the shape of the overall D-banding between the images taken of the microribbons [10] using AFM and the images produced during this report, these could probably be described by the differences in sample type and preparation. Continued comparison between these results and the AFM images of the microribbons as well as those taken using electron microscopy would be recommended, especially in conjunction with comparisons to variations in the microfibrillar packing model.

As the samples being used in the x-ray diffraction imaging are now being kept in liquid cells, further investigation into the banding shape and how it changes in liquid would be important. For this purpose, the use of sharper tips in intermittent contact mode would be recommended, as intermittent contact mode produces images of higher resolution in a liquid environment [8]. The phase signal could also be used qualitatively to investigate the variation of the viscoelastic properties in liquid.

Another important area that should be focused on is the further investigation of histological sections of collagen with respect to force-volume measurements. Unfortunately the sections that were provided for my imaging purposes were too strongly affected by the histology protocol – the fibrils were noticeably fatter, which may well be due to the picric acid used in the Van Gieson stain used on the section and there were obvious areas of wax that had not been fully removed. Also, the standard protocol that uses aldehydes to fix the sample will change the mechanical properties of the sample, making the force-volume measurements irrelevant to the native mechanical structure of collagen. To rectify this, cryo-sectioned specimens were asked for, but there was unfortunately no time to investigate these samples before the end of the project. The quality of the fibril cross-sections produced may also be a little hit-and-miss due to the uncertainty of the sample direction when sectioning. If these measurements were successful, then conclusions may be able to be drawn with regard to the internal structure and mechanics of the fibril, which is still contested.

Appendix 1

Cantilever tuning

Intermittent contact mode

- Prism is cleaned using ethanol and (scientific tissues)
- Desired tip is taken from gel-pack using tweezers and rested between the grooves on the slanted, matte area of the prism; a small part of the chip where the cantilever is situated should overhang onto the transparent part of the prism
- S-shaped spring is used to attach the chip to the prism, while still giving it some freedom of movement
- The AFM head with the cantilever in place is then rested on top of the AFM base, which is set on top of a gas floated table. The base has an integrated confocal microscope with camera, which is used to align the tip and sample as well as the laser and cantilever end.
- The laser is aligned first using the camera attached to the microscope, which is linked to the SPM software; when the tip has been found and is in focus, the laser is moved until it can be seen to be shining on the end of the cantilever (above the tip). The software window representing the photodiode is then brought up and the laser is again moved until the "sum" of the energy incident on it is at a maximum (this must at least be > 2V). If the sum energy stays obstinately low, then the mirror may have to be moved – this happens when going between imaging in liquid and in air due to refraction
- Finally the photodiode is aligned with the laser such that the laser spot is in the centre, at the point of intersection between the four photodiode panels
- When the laser is aligned, the cantilever is ready to be tuned. When calibrating the cantilever for intermittent contact, the software sets the cantilever in motion out of contact with the sample. On the calibration window, a frequency (between two values set by the experimenter, knowing the resonant frequency range for the specified cantilever) against oscillatory amplitude. The resonant peak is highlighted and zoomed in on, the experimenter then asks to see the phase shown on the same graph. The phase change is then altered until a high negative phase gradient coincides with a frequency just below the resonant frequency, where the driving frequency will be set. The amplitude setpoint should then be set at about 70% of the maximum amplitude (apex of resonant peak).
- The tip can now approach and engage with the sample, although the cantilever may need to be retuned just out of contact, so that the tip is experiencing *some* interaction when forced into oscillation. This is especially important for the high-resolution tips, as they are particularly affected by the interaction with the sample.
- After engaging with the sample, one can begin imaging. After this, the setpoint, gains, line rate, scan angle an z-range should be adjusted so as to gain the best possible image.

Contact Mode

- The AFM is prepared, the tip attached and the laser aligned as described for intermittent contact mode, but in place of a sample, a clean glass substrate should be in place. If the imaging is to be performed in liquid, then the liquid to be used should be deposited on the glass, as well as being carefully pipetted underneath the cantilever so that it is not broken by the surface tension of the liquid on the substrate surface. If force spectroscopy work is to be performed the cantilever should always be tuned in dry conditions before going into the liquid environment.
- The software is switched onto force spectroscopy mode and the experimenter asks the tip to approach the surface. After setting the parameters to the desired levels the software should be 'run'. This will give repeated force curve measurements. After checking that the force curve is of the correct shape, the calibration manager can be used to select the 'extend' curve, which is used to evaluate the sensitivity of the cantilever.
- After the sensitivity has been accepted the tip should be retracted and forced into oscillation again using the calibration manager, which can then be used to evaluate the resonance curve and accept a resonant frequency.
- After switching the software back to the contact imaging mode (either "in fluid" or "in air" depending on the imaging conditions) one can begin imaging, adjusting the setpoint, gains, z-range and line frequency so as to gain the best image. When imaging in liquid the line frequency should be lower than in air.

Appendix 2

Tips used

MikroMasch NSC15/Cr_Au BS Cantilever[2]

CANTILEVER

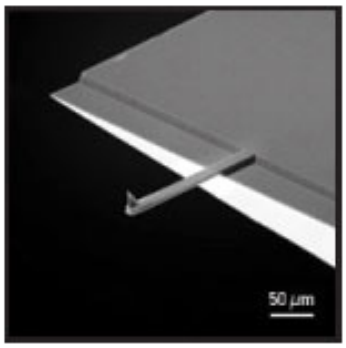

SEM image of Silicon cantilever and probe.

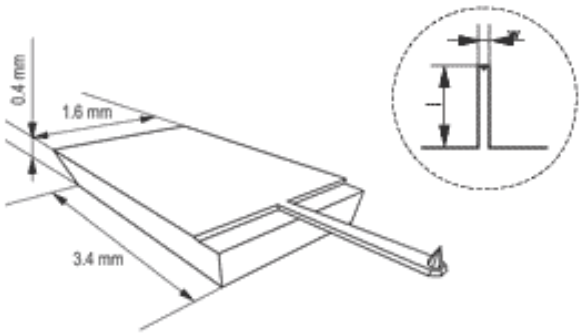

Schematic drawing of the probe chip.

Cantilever	Resonant Frequency, kHz			Spring Constant, N/m			Length l ± 5, µm	Width w ± 3, µm	Thickness t ± 0.5, µm
	min	**typ**	max	min	**typ**	max			
15 Series	265	**325**	400	20	**40**	75	125	35	4.0

[2] http://www.spmtips.com/nsc/15

NSC15

PROBE

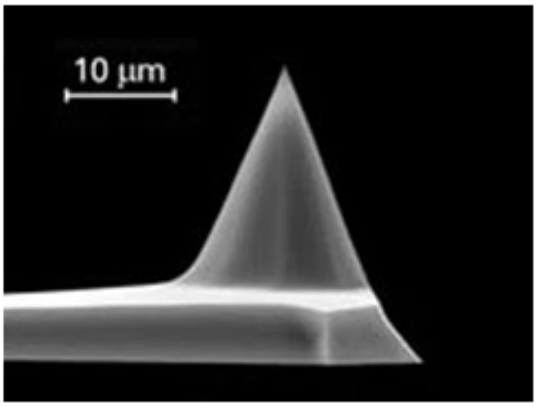

SEM image of uncoated silicon SPM probe tip

Silicon etched probe tip of the NSC series has a conical shape.

Typical probe tip radius of uncoated tip
10 nm

Full tip cone angle*
40°

Tip aspect ratio
more than 3:1 (4:1 typical)

Total tip height
20..25 µm

Probe material
n-type silicon (phosphorus doped)

Probe bulk resistivity
0.01..0.05 Ohm*cm

*The full cone angle may be less than 40° at the last 200 nm of the tip end.

Veeco DNP tip and cantilever[3]

Tip Specification

Geometry:	Cast
Tip Height (h):	2.5 - 3.5µm
Front Angle (FA):	35 ± 2°
Back Angle (BA):	35 ± 2°
Side Angle (SA):	35 ± 2°
Tip Radius (Nom):	20nm
Tip Radius (Max):	40nm
Tip SetBack (TSB)(Nom):	4µm
Tip Set Back (TSB)(RNG):	3 - 5.5µm

Cantilever Specification

DNP probes have less than 2deg of cantilever bend. The nominal stress specification for NP probes is less than 4deg of cantilever bend. For Veeco's Dimension SPMs, DNP is recommended.

Material:	Silicon Nitride
Thickness (t)(Nom):	0.6µm
Thickness (t)(RNG):	0.4 - 0.7µm
Back Side Coating:	—
Bottom Layer Back:	15nm of Cr
Top Layer Back:	60nm of Au

[3] http://www.veecoprobes.com/p-3588-dnp.aspx

Appendix 3

JPK NanoWizard® II AFM sample stage and AFM head

Sample stage: sample holder, adjustable in x,y-plane

AFM head: incorporating piezo tube, laser and photodiode. Prism for cantilever mounting is exposed

Entire microscope body incorporating confocal microscope – Olympus set-up.

Appendix 4[4]

Kapton®

Kapton® is a polyimide film developed by DuPont, used over a wide range of industries from aerospace to flexible printed circuits. It has been widely used at x-ray sources as it is highly resistant to radiation damage and has a high x-ray transmittance.

[4] http://www2.dupont.com/Kapton/en_US/

References

1. *Topography and mechanical properties of single molecules of type I collagen using AFM*, Bozec & Horton, Biophysical Journal 88:4223-4231, 2005
2. *UNPUBLISHED: Coherent x-ray diffraction from collagenous soft tissues,* Berenguer, Wenger, Bean, Bozec, Horton, Robinson, dated 08/12/2008
3. *Testing the feasibility of using ptychographical methods in determining the structure of the D-banding from rat-tail tendon collagen*, Kris Wallace, MSci project, 2009
4. www.sbes.v.edu/freeman/research/collagen_modeling.html
5. *Cellular remodelling of individual collagen fibrils visualised by time-lapse AFM,* Friedrichs, Taubenberger, Franz, Müller, Journal of Molecular Biology 372:594-607, 2007
6. *Collagen,* Jürgen Brinckmann, Holger Notbohm, P. K. Müller, 2005
7. *Biochemsitry of Collagen,* Ramachandran & Reddi, 1976
8. *Observing growth steps of collagen self assembly by time lapse high resolution AFM,* Cisernos, Hung, Franz, Müller, Journal of structural biology 154:232-245, 2006
9. *In vitro reconstitution of fibrillar collagen type I assemblies at reactive polymer surfaces,* Salchert Strellar, Pompe et al., Biomacromolecules 5:1340-1350, 2004
10. *The interpretation of electron micrographs of negatively stained native collagen,* Cox, Grant, Kent, Journal of cellular science 10:547-554, 1972
11. *Microfibrillar structure of type I collagen **in situ**,* Orgel, Irving, Miller, Wess, PNAS vol. 13, no. 24:9001-9005, 2006
12. *The multicomposite structure of tendon,* Kastelic, Galeski, Baer, Connective Tissue Research, Vol. 6, Issue 1, 1978; 11-23
13. *Atomic Force Microscopy for Biologists,* Morris, Kirby, Gunning; ISBN 1-86094-199-0
14. *Springer Handbook of Nanotechnology* Bharat Bhushan, Springer ISBN: 3-540-01218-4
15. *Deformation, contact time and phase contrast in intermittent contact mode scanning force microscopy,* Tamayo & Garcia 1996
16. *Physics for Scientists and Engineers with Modern Physics,* Serway, Jewett; ISBN 0-534-40949-0
17. *TipCheck:* www.budgetsensors.com/tip-check.html
18. *Hard x-ray lensless imaging of extended objects,* Rodenburg et. al., Physical Review Letters 98, 034801 (2007)
19. *Basic Histology: Text and Atlas,* Luiz Carlos Uchôa Junqueira & José Carneiro, McGraw Hill Medical, ISBN: 0-07-144091-7
20. Private communication, P. Darkins (*Histologist, Eastman Dental Institute)*
21. *Diamond Light Source:* http://www.diamond.ac.uk/default.htm (http://www.diamond.ac.uk/Beamlines/Beamlineplan/I22/TechSpecs.htm)
22. *Gwyddion opensource software:* http://gwyddion.net
23. *Structural Heterogeneity in tendon Collagen from Different Sources,* Patricia Almlof, CoMPLEX MRes Summer Project, 2005
24. *Glycation changes the charge distribution of type I collagen fibrils,* Hadley, Meek, Malik, Glycoconjugate Journal 15:835-840, 1998
25. *A study of fibrous long spacing collagen ultrastructure and assembly by AFM,* Paige, Rainey, Goh, Micron 32:341-353, 2001
26. *Investigating the ultrastructure of fibrous long spacing collagen by parallel AFM and TEM*, Lin & Goh, **Proteins:** structure, functions and genetics 49:378-384, 2002

27. *Image analysis of mineralised and non-mineralised type I collagen fibrils,* Arsenault, Journal of electron microscopy technique 18:262-268, 1991